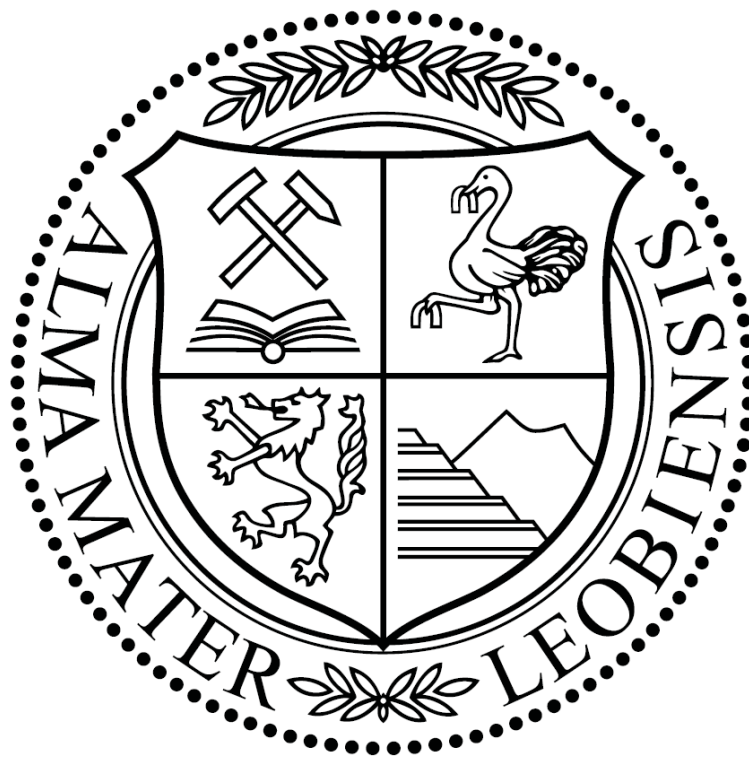**Montanuniversität Leoben**

Characterization of an orthorhombic phase in a water-quenched Ti-44Al-3Mo (at.%) alloy using *in situ* synchrotron diffraction and transmission electron microscopy

Michael Musi

Department of Physical Metallurgy and Materials Testing,

Montanuniversität Leoben

September 2018

Affidavit:

I declare in lieu of oath, that I wrote this thesis and performed the associated research myself, using only literature cited in this work.

Leoben, September 2018   Signature

Acknowledgement

Table of contents

List of abbreviations

abs .... absolute

Al....................... Aluminum

at.%.................... Atomic percent

B........................ Boron

bcc .... body-centered cubic

HEXRD................ High-energy X-ray diffraction

HIP .... Hot isostatic pressing

Mo .... Molybdenum

Nb .... Niobium

RT...................... Room temperature

SEM.................... Scanning electron microscopy

TEM.................... Transmission electron microscopy

TiAl.................... Titanium aluminide

TNB .... γ-titanium aluminide alloy containing Nb (e.g. Ti-46Al-9Nb (at.%))

TNM................... γ-titanium aluminide alloy containing Nb and Mo: Ti-43.5Al-4Nb-1Mo-0.1B

(at.%)

vol.% .... Volume percent

_____

Abstract/Kurzfassung

Abstract

In this work the thermally activated formation of an orthorhombic phase in a β-homogenized and water-quenched Ti-44.5Al-3.2Mo-0.1B (at.%) alloy is studied. The goal was to identify the type of this orthorhombic phase and to investigate the temperature interval of its formation and dissolution as well as its phase stability. For this purpose, *in situ* heating and ageing high-energy X-ray diffraction experiments starting from the water-quenched state were carried out at the synchrotron radiation source PETRA III at the DESY in Hamburg, Germany. Additionally, scanning and transmission electron microscopy was used to study the evolution of the microstructure at different length scales.

During the reheating of the β-homogenized and water-quenched samples the splitting of the α_2 peaks could be observed in a temperature range from 590 °C to 724 °C in the synchrotron data. This could be attributed to the formation of an orthorhombic phase, which consumed a significant amount of α_2 phase. Using Rietveld analysis, the synchrotron data were evaluated to characterize the formed orthorhombic phase in terms of lattice parameters and phase fraction. After exceeding 724 °C the orthorhombic phase vanished and a large amount of γ phase formed. The *in situ* heating and cooling experiments showed that the orthorhombic phase only formed upon reheating after the water quenching and not during a subsequent cooling. In combination with the formation pathway $\alpha_2 \rightarrow$ orthorhombic phase$\rightarrow\gamma$ it could be concluded that the orthorhombic phase is a metastable transition phase between the α_2 and the γ phase for this type of alloy. Furthermore, higher heating rates lead to the shift of the formation and dissolution of the orthorhombic phase to higher temperatures. Using Rietveld refinement on the basis of the implemented structural phase models the lattice parameters could be evaluated. All of them were in good agreement with literature.

The TEM investigation revealed that after water quenching from the β single-phase field region the microstructure mainly consisted of large α_2 laths with a mixture of α_2' martensite and β_o phase in between. Upon the reheating process the orthorhombic phase precipitated in the form of small lamellae within the α_2 laths and the α_2' martensite. After

exceeding the dissolution temperature of the orthorhombic phase, the γ phase formed fine lamellae, similar to the orthorhombic phase, within the α_2 laths and the α_2' martensite.

Kurzfassung

Diese Arbeit setzt sich mit der thermisch aktivierten Bildung einer orthorhombischen Phase in einer β-homogenisierten und wasserabgeschreckten Ti-44.5Al-3.2Mo-0.1B (at.%) Legierung auseinander. Das Ziel war es den Typ der orthorhombischen Phase zu identifizieren und deren Bildungs- und Auflösungs-Temperatur sowie die Phasenstabilität zu untersuchen. Dafür wurden *in situ* Aufheiz- und Auslagerungs-HEXRD-Experimente ausgehend von den wasserabgeschreckten Proben an der Synchrotron-Quelle PETRA III am DESY in Hamburg, Deutschland, durchgeführt. Zusätzlich wurden Raster- und Transmissions-elektronenmikroskopie verwendet um die Veränderungen des Gefüges auf unterschiedlichen Längenskalen zu studieren.

Während des Aufheizens der β-homogenisierten und wasserabgeschreckten Proben konnte eine Aufspaltung der α_2 Peaks in einem Temperaturbereich von 590 °C bis 724°C beobachtet werden. Dies konnte der Bildung einer orthorhombischen Phase zugeschrieben werden. Mit Hilfe einer Rietveld-Analyse wurden die Synchrotron-Daten ausgewertet um die gebildete orthorhombischen Phase im Hinblick auf ihre Gitterkonstanten und ihren Phasenanteil zu charakterisieren. Nach dem Überschreiten von 724°C während der Aufheizexperimente kam es zur Auflösung der orthorhombischen Phase und zur Bildung einer großen Menge an γ Phase. Die *in situ* Aufheiz/Kühlversuche zeigten außerdem, dass sich die orthorhombische Phase nur während des Heizens nach dem Wasserabschrecken bildet. In Kombination mit der Bildungssequenz $\alpha_2\rightarrow$orthorhombische Phase$\rightarrow\gamma$ wurde gefolgert, dass es sich bei der orthorhombischen Phase um eine metastabile Zwischenphase zwischen α_2 und γ handeln muss. Versuche bei höheren Heizraten zeigten, dass sich sowohl die Bildung als auch die Auflösung dieser Phase zu höheren Temperaturen verschoben hatten. Mit Hilfe einer Rietveldanalyse auf Basis der implementierten Phasenmodelle konnten auch die Gitterkonstanten der vorhandenen Phase ausgewertet werden, welche sehr gut mit Literaturwerten übereinstimmten.

Die TEM-Untersuchungen zeigten, dass nach dem Wasserabschrecken das Gefüge aus großen α_2 Latten und einer Mischung aus α_2' Martensit und β_o Phase dazwischen bestand. Während der *in situ* Versuche bildete die orthorhombische Phase Lamellen in der α_2 Phase und dem α_2' Martensit. Nach der Auflösung der orthorhombischen Phase bildete die γ Phase ebenfalls Lamellen in der α_2 Phase und dem α_2' Martensit.

_____

Introduction

Intermetallic γ-TiAl based alloys offer outstanding properties, such as a high specific strength and stiffness, good oxidation resistance and high creep resistance. This makes them favorable for applications in the aerospace and automotive industry [1]. Nowadays, already the 3rd generation of these alloys is available. Two examples are the TNM alloy and the TNB alloy. Beside the main elements titanium and aluminum they contain various further alloying elements to tune their properties with respect to their applications. Important alloying elements are molybdenum and niobium [1,2]. The nominal TNM alloy contains 4 at.% niobium and 1 at.% molybdenum - hence the name TNM -, whereas the TNB alloy can be alloyed with up to 10 at.% niobium [3]. These β-stabilizing elements are, for example, used to increase the creep resistance and the strength [1,3–5]. However, under certain circumstances the addition of these elements can lead to the formation of phases, which do not occur in the binary Ti-Al system. In literature, different phases can be found for this type of alloys, for example ω/ω_o-related phases and orthorhombic phases [6–8]. The latter ones are of great importance for this work. In recent years, a growing body of literature has examined the orthorhombic B19 phase and the orthorhombic O phase [7,8].

This thesis deals with the formation of an orthorhombic phase in a Ti-44.5Al-3.2Mo-0.1B (at.%) alloy, which forms upon reheating after water quenching from the β single-phase field region. This phase is investigated with the help of _in situ_ high-energy synchrotron X-ray diffraction regarding its formation and dissolution behavior and its phase stability. Furthermore, phase fractions, lattice parameters as well as site occupancy factors are evaluated with a Rietveld analysis of the synchrotron diffraction data. Scanning and transmission electron microscopy are used to study the evolution of the microstructure at different length scales. It should be mentioned that most of the results of this work will be/have been published in the form of a paper, which is attached in the appendix. This Master thesis complements the published paper by going more into detail, especially in the theoretical part. The first section of the theoretical part covers the Ti-Al-Mo system and outlines the effects of molybdenum on the occurring phases. The second section describes the orthorhombic phases in detail. Their crystal structures are shown and the differences explained. Additionally, alloying systems, in which the formation of these phases has been

reported, are mentioned. The last section of the theoretical part deals with the martensitic transformation in TiAl alloys, and the different types of martensite are outlined. The main part mostly refers to the results and discussion section of the paper. However, the evolution of the phase fractions with time and temperature during the *in situ* measurements is shown. Furthermore, more supplementary figures regarding the splitting of the α_2 peaks are given in this section.

_____

The Ti-Al-Mo system

2.1 The effects of molybdenum on the binary Ti-Al system

Figure 1a shows the binary phase diagram of titanium and aluminum and the red line indicates an aluminum content of roughly 44 at.%. For such a γ-TiAl based alloy various phases can occur depending on the temperature. When cooling from the liquid single-phase field the disordered cubic β-Ti(Al) phase begins to form out of the liquid at the liquidus temperature. Depending on the exact aluminum content two possible solidification pathways arise. A binary alloy with an aluminum content below roughly 44 at.% solidifies completely via the β phase, which yields almost no segregations and solidification texture [9]. Alloys with an aluminum content above approximately 44 at.%, however, solidify via a peritectic transformation of the liquid and the β phase into the disordered hexagonal α-Ti(Al) phase. This transformation path results in the formation of macroscopic columnar grains and pronounced microsegregations [4]. However, as the red line in Fig. 1a indicates, this peritectic transformation only leads to the formation of a small amount of α phase for 44 at.% aluminum. After the (α+β) phase field the system enters the α single-phase field upon further cooling. At the γ-solvus temperature the ordered face-centered γ-TiAl phase precipitates from the α phase. At the eutectoid temperature the remaining part of the α phase transforms into the γ phase and ordered hexagonal α_2-Ti₃Al phase via an eutectoid reaction. The α_2 and the γ phase are stable phases at low temperatures.

The alloying with molybdenum now results in a large change in the phase diagram. The effect of molybdenum on a binary TiAl alloy with 44 at.% aluminum can be seen in Fig. 1b. There the quasi-binary phase diagram for such an alloy is shown in dependence of the molybdenum content. Due to the β-stabilizing effect of molybdenum the β phase is stabilized at lower temperatures. Furthermore, the disordered β phase shows an ordering transformation into the ordered bcc β_o-TiAl phase during cooling. For a molybdenum content of 3 at.% this ordering reaction occurs at 1240 °C, as was found by Schmoelzer et al. [10]. If the molybdenum content becomes high enough, stabilization of the β_o phase at room temperature is possible. Additionally, molybdenum shows a strong partitioning behavior between the phases. It prefers to enrich in the β/β_o phase because of its strong β-stabilizing

character [11]. Another consequence of the alloying with molybdenum and other β-stabilizing elements is the formation of orthorhombic phases, which has been widely reported in literature [7,8,12–15]. These orthorhombic phases are described in detail in chapter 3.
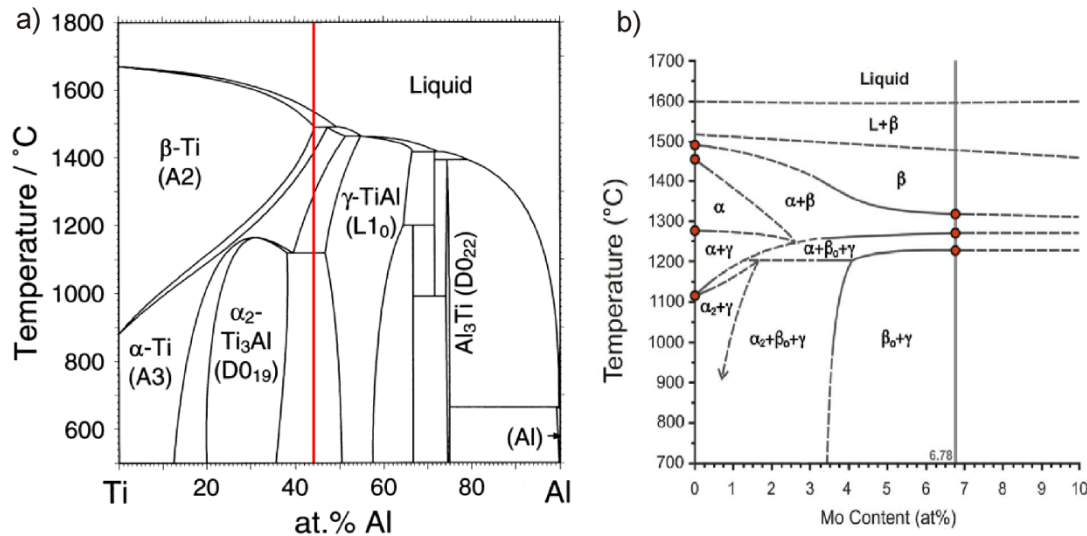
Fig. 1: (a) Binary phase diagram of titanium and aluminum after Ref. [16]. Reprinted from Acta Materialia, 48, I. Ohnuma, Y. Fujita, H. Mitsui, K. Ishikawa, R. Kainuma, K. Ishida, Phase equilibria in the Ti-Al binary system, 3113-3123, Copyright (2000), with permission from Elsevier. The red vertical line indicates an alloy with 44 at.% aluminum; (b) quasi-binary phase diagram of a Ti-44Al-(0-10)Mo (at.%) alloy (at.%) after Ref. [17]. Reprinted from Materials Science and Engineering: A, 700, L. Usategui, M.L. Nó, S. Mayer, H. Clemens, J. San Juan, Internal friction and atomic relaxation processes in an intermetallic Mo-rich Ti-44Al-7Mo (γ+β$_o$) model alloy, 495-502, Copyright (2017), with permission from Elsevier.

2.2 The lattice structure of the main equilibrium phases

For the evaluation of the synchrotron diffraction data with a Rietveld analysis the structural parameters of each phase are of great importance. The lattice parameters of the main equilibrium phases, which were used as initial values in the Rietveld analysis, can be found in Tab. 1. The crystal structures of the equilibrium phases are shown in Fig. 2. Beside the lattice parameters and the space groups, the knowledge of the positions of the individual atoms in the unit cells is mandatory. These positions can be found in Ref. [18]. For this thesis the α$_2$ phase, the β$_o$ phase and the γ phase are essential because they are the only occurring equilibrium phases during the diffraction experiments.

Tab. 1: Structural parameters of the equilibrium phases. For each phase the alloying system is shown, for which the lattice parameters have been determined. The lattice parameters of α and β were taken from Ref. [19], the ones of α_2 and γ from Ref. [20] and the one of β_o from Ref. [21]. The space groups were taken from Ref. [20].

	α-Ti(Al)	**α_2-Ti$_3$Al**	**β-Ti(Al)**	**β_o-TiAl**	**γ-TiAl**
Space group	P63/mmc	P63/mmc	Im-3m	Pm-3m	P4/mmm
Alloy	High-purity Ti	Ti-25Al (at.%)	High-purity Ti	Ti-44Al-2Mo (at.%)	Ti-50Al (at.%)
Lattice parameters in [Å]	a = 2.95 a = 4.68	a = 5.765 a = 4.625	a = 3.32	a = 3.21	a = 4.016 a = 4.068
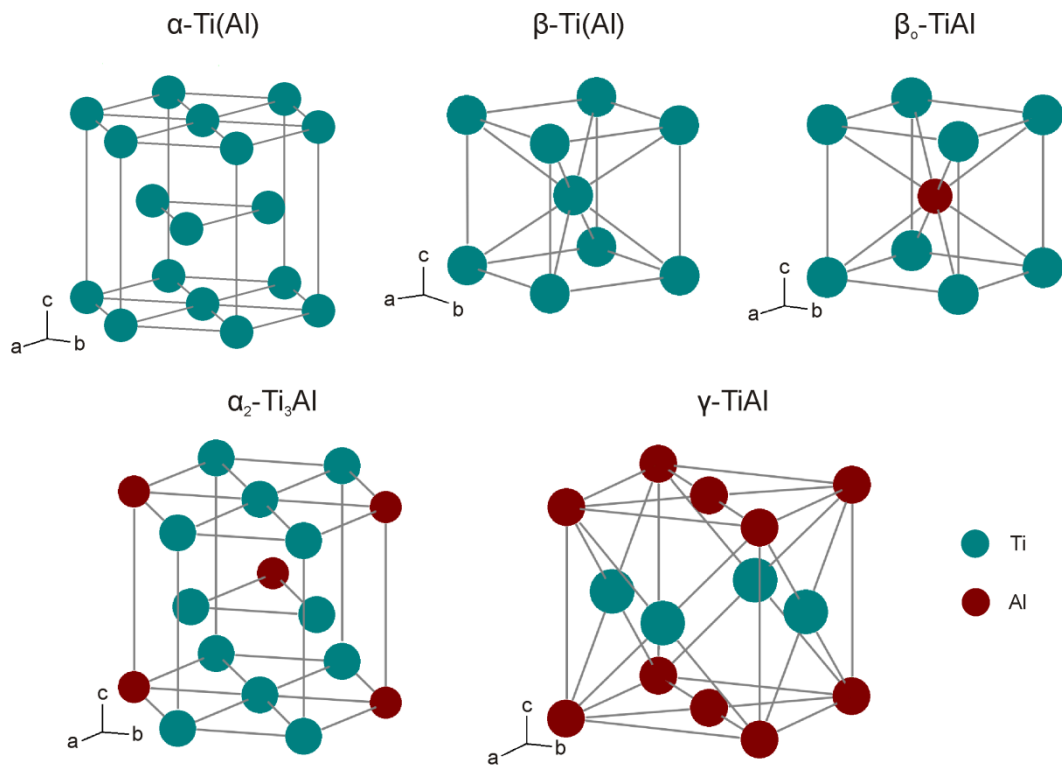
Fig. 2: Unit cells of the equilibrium phases.

The α_2 phase has an ordered hexagonal structure (D0$_{19}$ structure) as shown in Fig. 2 and is formed via the ordering of the α phase (A3 structure), its high-temperature counterpart [18]. Even at the highest cooling rates this ordering cannot be suppressed [4]. Regarding X-ray diffraction the ordered structure yields the occurrence of superstructure peaks in the diffraction data. These peaks are forbidden reflexes in the disordered structure, where the X-rays diffracted by the lattice planes interfere destructively. In the ordered structure these waves do not cancel each other completely because of the order structure and, therefore, the superstructure reflections can be observed.

The γ phase shows an ordered face-centered L1$_0$ structure, which can be described by the stacking of alternating titanium and aluminum planes in the [001] direction [18]. The unit cell, which is shown in Fig. 2, is tetragonally distorted in the c-direction. This distortion, however, is rather small with a c/a ratio of 1.02 at the equiatomic composition [22]. Similarly

to the α_2 phase the ordered structure leads to the occurrence of superstructure peaks. The γ phase and the α_2 phase can form lamellar colonies, where the two phases exhibit a certain orientation relationship. This orientation relationship, which is called Blackburn orientation relationship, is given below [23].

$$(0001)_{\alpha_2} \parallel (111)_{\gamma} \qquad\qquad \langle 11\bar{2}0\rangle_{\alpha_2} \parallel \langle 1\bar{1}0]_{\gamma} \qquad\textbf{(Eq. 1, 2)}$$

Equation 1 shows that the close-packed planes are parallel, whereas Eq. 2 describes that the close-packed directions of both phases are parallel. The γ phase as well as the α_2 phase show a rather brittle behavior when used as a single-phase alloy. The combination of both, however, yields much better mechanical properties [3,11]. So in modern 3rd generation γ-TiAl based alloys the microstructure mainly consists of γ and α_2 phase. In the TNM alloy, for example, with a two-step heat treatment lamellar α_2/γ colonies are formed, which are surrounded by globular γ and β_o grains. Such a microstructure provides balanced mechanical properties [3].

The β_o phase has an ordered bcc structure (B2 structure), where the aluminum atom e.g. sits in the middle of the unit cell and the titanium atoms at the corners, as shown in Fig. 2 [18]. Also for this phase superstructure peaks occur due to its ordered nature. Although β_o is not beneficial for the high-temperature application due to its poor creep resistance, it is important for the processing of β-stabilized γ-TiAl based alloys. Since its disordered counterpart, the β phase (A2 structure), is stable at elevated temperatures, a large improvement of the hot-workability can be achieved [3,11].

At the beginning of this section the great importance of the structural parameters for the Rietveld analysis was mentioned. Also the atomic positions within the unit cells are needed for the phase models. The α_2, the β_o and the γ phase have one titanium sublattice each. The α_2 and β_o phase possess one aluminum lattice, whereas the γ phase possesses two [6]. But since the studied alloy contains 3 at.% of molybdenum, the question arises, how this element should be distributed on the different sublattices. Holec et al. [24] have performed first principle calculations regarding the preferential site occupancy of the early transition metals in different TiAl-based phases. For the α_2 and γ phase molybdenum tends to occupy the titanium sublattice. In the β_o phase, however, it prefers the aluminum sublattice [24].

_____

Orthorhombic phases in TiAl alloys

Orthorhombic phases have a crystal structure, in which all unit cell vectors share an angle of 90° but have a different length. This gives rise to the three lattice parameters a, b and c. Orthorhombic phases tend to form in γ-TiAl based alloys with a high amount of β-stabilizing elements like molybdenum and niobium [7,8,12–15]. However, also for binary and ternary TiAl alloys these phases were reported in literature [25,26]. The following chapter deals with two orthorhombic phases, called B19 phase and O phase, which are reported frequently in literature. Their structural parameters are shown and the differences between these phases are outlined. Alloys are mentioned where these phases occur and possible formation paths are described.

3.1 The B19 phase

3.1.1 Structure of the B19 phase

The unit cell of the B19 phase is shown in Fig. 3a, and the structural parameters are given in Tab. 2. The B19 phase belongs to the space group Pmma and shows an orthorhombic symmetry. It can be described as the ABAB stacking of γ-(111) planes, which are close-packed planes due to the face-centered character of the γ phase. The B19 phase can, therefore, be interpreted as a transition state between the γ phase, where the stacking of the (111) planes follows the pattern ABCABC, and the hexagonal α_2 phase, because of the ABAB stacking [18]. Regarding XRD this has a major consequence. Because of the structural similarity between the B19 and the α_2 phase their reflections tend to show a large overlap [8]. The similarities between these two phases, but also between the γ and the B19 phase, become even more obvious, when the close-packed planes of the three phases are compared, which are shown in Fig. 3b. Except for the different atoms on the lattice positions they share essentially the same close-packed planes. For the α_2 and the γ phase this leads to the already mentioned Blackburn relationship. So for the B19 phase a similar orientation relationship with the α_2 phase and, respectively, with the γ phase can be assumed.
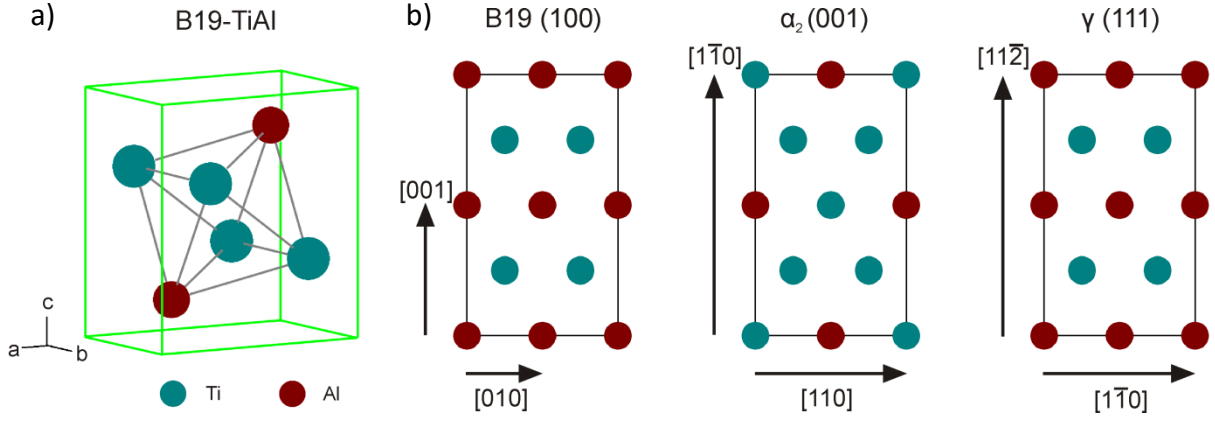
Fig. 3: (a) shows the unit cell of the B19 phase. In (b) the close-packed planes of the B19, the α_2 and the γ phase are shown. For each phase a pair of lattice vectors is shown, which define the close-packed plane.

Tab. 2: Structural parameters of the B19 phase. The lattice parameters at room temperature (RT) were taken from Ref. [25] for a Ti-48Al (at.%) alloy and at 640 °C from Ref. [8] for a Ti-44.6Al-3.2Mo-0.1B (at.%) alloy. The lattice occupation of the elements was taken from Ref. [18].

Lattice parameters in [Å]			Lattice occupation				
	RT	640 °C	Element	Wyckoff pos.	Atomic coordinates (x, y, z)		
a	4.5	4.65	Ti	2e	1/4	0	z=1/3
b	2.8	2.93	Al	2f	1/4	1/2	z=5/6
c	4.9	4.95					

This orientation relationship leads to the possibility of calculating "ideal" lattice parameters of the B19 phase. It is assumed that the atomic distances on the close-packed plane of the B19 phase are essentially the same as in the α_2 and the γ phase. The comparison of the horizontal lattice vectors in Fig. 3b for the phases yields Eq. 3-6.

$$2 * |[010]_{B19}| = \left|[110]_{\alpha_2}\right| \qquad\qquad 2 * |[010]_{B19}| = \left|[1\bar{1}0]_{\gamma}\right| \qquad \textbf{(Eq. 3, 4)}$$

$$b_{B19} = \frac{1}{2}a_{\alpha_2} \qquad\qquad\qquad b_{B19} = \frac{\sqrt{2}}{2}a_{\gamma} \qquad \textbf{(Eq. 5, 6)}$$

An analog calculation can be made for the vertical vectors, which yields an expression for the lattice parameter c of the B19 phase (Eq. 7-10).

$$2 * |[001]_{B19}| = \left|[1\bar{1}0]_{\alpha_2}\right| \qquad\qquad 2 * |[001]_{B19}| = \left|[11\bar{2}]_{\gamma}\right| \qquad \textbf{(Eq. 7, 8)}$$

$$c_{B19} = \frac{\sqrt{3}}{2}a_{\alpha_2} \qquad\qquad\qquad c_{B19} = \frac{1}{2}\sqrt{2a_{\gamma}^2 + 4c_{\gamma}^2} \qquad \textbf{(Eq. 9, 10)}$$

As the lattice vectors [100] and [010] are not perpendicular in the hexagonal lattice of the α_2 phase, the length of the [1$\bar{1}$0] vector was derived via geometric considerations. For the lattice parameter a of the B19 phase some further assumptions have to be made. Since all three phases can be described as a different type of stacking of close-packed planes, it can

be assumed that the atomic packing factors are the same. Therefore, the unit cells must have the same volume. With this assumption the lattice parameter a can be calculated. This only works, however, if the unit cells contain the same amount of atoms. In the case of the B19 and γ phase the number of atoms per unit cell is four, whereas in the α_2 phase it is eight. So the volume of the α_2 unit cell has to be divided by two (Eq. 11-14).

$$V_{B19} = \frac{1}{2}V_{\alpha_2} \qquad\qquad V_{B19} = V_{\gamma} \qquad\text{(Eq. 11, 12)}$$

$$a_{B19} = \frac{\sqrt{3}*a_{\alpha_2}^2*c_{\alpha_2}}{4*b_{B19}*c_{B19}} \qquad\qquad a_{B19} = \frac{a_{\gamma}^2*c_{\gamma}}{b_{B19}*c_{B19}} \qquad\text{(Eq. 13, 14)}$$

Table 3 shows the results for the calculated lattice parameters of the B19 phase when using the α_2 and the γ lattice parameters from Ref. [20] (see Tab. 1) and those determined in the present work (see Tab. 2 in the appended paper). They are all in a good agreement with the experimentally determined lattice parameters in Tab. 2. In the lower part of Tab. 3 the deviation of the calculated constants from the ones determined by Abe et al. [25] (a=4.5 Å, b=2.8 Å, c=4.9 Å) and the ones determined in the present work (a=4.615 Å, b=2.920 Å and c=4.889 Å) is shown by means of the sum of the absolute errors. When comparing the deviations of the calculated lattice parameters from the ones determined by Abe et al. [25] and from the ones that stem from the present work, it can be seen that the former deviations are larger than the latter ones. A possible source of errors are the differences in the chemical compositions of the alloys, in which the lattice parameters have been determined. Also the assumptions necessary for the derivation of Eq. 3-14 may lead to errors. This is reflected, in particular, in the difference between the calculated B19 lattice parameters in columns 2 and 4 in Tab. 3 and the ones determined experimentally in the present work. For these the difference in the chemical composition is negligible, and, therefore, the deviations of the calculated lattice parameters from the ones determined experimentally are smaller. Using the lattice parameters of the α_2 phase yields a better agreement with the literature values in three out of four cases.

Tab. 3: In the upper part the lattice parameters of the B19 phase are shown that were calculated using the lattice parameters of the α_2 and the γ phase from Ref. [20] and from the present work. The lower part shows the sums of the absolute errors for each set of the calculated lattice parameters when compared with the ones determined by Abe et al. [25] and the ones determined in the present work.

			Using the α_2 lattice parameters		Using the γ lattice parameters	
			After Ref. [20]	Present work	After Ref. [20]	Present work
Lattice parameters of the B19 phase [Å]		a	4.624	4.616	4.657	4.693
		b	2.883	2.874	2.840	2.867
		c	4.993	4.978	4.961	4.991
Sum of abs. errors [Å]	From Ref. [25]		0.30	0.27	0.26	0.35
	Present work		0.15	0.14	0.19	0.23

3.1.2 Alloying systems

The first researchers to report on the B19 phase in a TiAl alloy were Abe et al. [25]. They found that the B19 phase formed after a rapid cooling from the α region in a binary Ti-48Al (at.%) alloy. It precipitated with a size of less than 200 nm in the α_2 phase. Tanimura et al. [26] found the B19 phase also in a binary alloy after quenching from 1250 °C. However, the chemical composition of the studied alloy was Ti-40Al (at.%). The B19 phase occurred as a metastable transition phase, which formed in the α/α_2 phase and acted as nucleation site for the γ formation during a subsequent annealing. So Abe et al. [25] as well as Tanimura et al. [26] observed the B19 phase after quenching from the α region.

Besides these binary TiAl alloys the B19 phase has also been reported for molybdenum- and niobium-containing γ-TiAl based alloys. With the help of HEXRD Schmoelzer et al. [10] found a transition phase during the reheating of a quenched Ti-45Al-3Mo-0.1B (at.%) alloy, which they could identify as an orthorhombic phase due to the splitting of the α_2 peaks. They suggested that the formed phase was the B19 phase, which was present in a temperature region from 600 °C to 700 °C. So in contrast to the binary alloys studied in Ref. [25] and [26], in which the B19 phase had formed during quenching, in the case of the molybdenum-containing γ-TiAl based alloy it had formed during reheating. However, similarly to the alloy investigated by Tanimura et al. [26], the B19 phase acted as a transition phase between α_2 and γ also in the alloy studied by Schmoelzer et al. [8].

In niobium-rich γ-TiAl based alloys the B19 phase is often part of a so-called modulated microstructure. This microstructure is characterized by fine lamellae, which show a contrast modulation when investigated with TEM. This modulation stems from a gradual change of the lattice structure [13]. Appel et al. [13,27,28] observed such a microstructure with the B19 phase in Ti-(40-44)Al-8.5Nb (at.%) alloys using TEM. Furthermore, they suggested that the B19 phase had formed via the decomposition of the B2 phase according to the transformation mechanism described by Nguyen-Manh et al. [29]. Song et al. [14] reported the B19 phase in a Ti-45Al-8.5Nb-0.2W-0.2B-0.02Y (at.%) alloy, in which it had formed inside the α_2 laths. This is in contrast to the findings of Appel et al. [13,27,28]. In the alloy studied by Song et al. [14] the B19 phase was unstable and could be eliminated after a short annealing. Using high-resolution TEM Ducher et al. [30] observed additional spots in the diffraction pattern of the γ phase in a 46.4Al–1.3Cr–1.8Nb–1.3Fe (at.%) alloy. With the help of simulation they could show that the B19 phase was responsible for these spots. But in contrast to Abe et al. [25] they found that the orthorhombic phase was incorporated within the γ phase and had formed domains rather than small precipitates.

So the literature shows that the formation of the B19 phase can be quite different for different alloys. Schmoelzer et al. [8], Abe et al. [25] and Tanimura et al. [26] found that the B19 phase had formed in the α_2 phase, although they did not investigated the same alloys.

On the other site, Appel et al. [13,27,28] proposed the formation of the B19 phase via the decomposition of the B2 phase in a niobium-containing γ-TiAl based alloy. This different transformation path might be possible because of the addition of niobium. However, this gives rise to the question, why in the case of the molybdenum-containing γ-TiAl based alloy studied by Schmoelzer et al. [8] the B19 phase had not formed from the β_o phase. Possible explanations are a different thermal history of the studied alloys and a different effect of molybdenum and niobium on the B19 phase. So although the existence of the B19 phase is well established in the Ti-Al system, further investigations regarding the chemical and the temperature regime are needed to fully understand the formation of this phase.

3.2 The O phase

3.2.1 Structure of the O phase

The O phase is a stable phase within the ternary Ti-Al-Nb system with a stoichiometric constitution of Ti_2AlNb and shows a Cmcm symmetry [18]. Its crystal structure is shown in Fig. 4a and its structural parameters are given in Tab. 4. The O phase is the other frequently mentioned orthorhombic phase in literature besides the B19 phase. Their crystal structures are very similar and the only difference is the occupation of the Wyckoff positions 4c1 and 4c2. In comparison to the B19 phase, where these are occupied equally, in the O phase the occupation is different for these two Wyckoff positions [7].
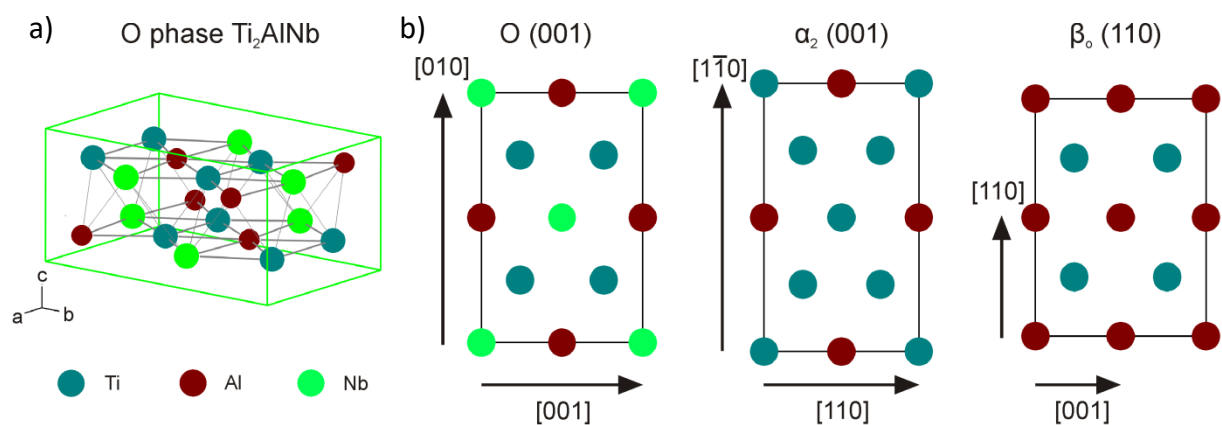
Fig. 4: (a) Unit cell of the O phase. In (b) the close-packed planes of the O, the α_2 and the β_o phase are shown. For each phase a pair of lattice vectors is shown, which define the close-packed plane.

Tab. 4: Structural parameters of the O phase. The lattice parameters were taken from Ref. [31] for a Ti-25Al-25Nb (at.%) alloy. The shown lattice occupation belongs to the O2 phase and was taken from Ref. [32].

Lattice parameters in [Å]		Lattice occupation				
	RT	Element	Wyckoff pos.	Atomic coordinates (x, y, z)		
a	6.09	0.82 Ti; 0.18 Nb	8g	x=0.231	y=0.904	1/4
b	9.57	Al	4c1	0	y=0.163	1/4
c	4.67	0.65 Nb; 0.35 Ti	4c2	0	y=0.636	1/4

It is worth noting that the O phase was found in two different forms, called O1 phase and O2 phase [32]. The difference between these two phases is the occupancy of the sublattices. In the case of the O1 phase the titanium and the niobium atoms are randomly distributed on the 8g and the 4c2 Wyckoff positions, whereas in the case of the O2 phase niobium mainly occupies the 4c2 positions and titanium the 8g positions. The transformation from the O1 into the O2 phase can be accomplished by a replacive ordering wave [32]. In general, the O phase is structurally closely related to the α_2 and β_o phase, which can be seen in Fig. 4, where the close-packed planes for these phases are shown [18]. The main differences are that different types of atoms occupy different positions within the lattice and that the interatomic distances are slightly different. When transforming the β_o phase into the α_2 phase an atomic shuffle and a shearing of lattice planes is needed. For the O phase this shuffle and shear is not completed, which makes it an intermediate state between the α_2 and the β_o phase [32,33].

Using the same procedure as with the B19 phase, it is possible to calculate some estimated lattice parameters for the O phase. This leads to the equations Eq. 15-20.

$$a_O = a_{\alpha_2} \qquad\qquad a_O = 2a_{\beta_o} \qquad \textbf{(Eq. 15, 16)}$$

$$b_O = \sqrt{3}a_{\alpha_2} \qquad\qquad b_O = 2\sqrt{2}a_{\beta_o} \qquad \textbf{(Eq. 17, 18)}$$

$$c_O = \frac{\sqrt{3}a_{\alpha_2}^2 c_{\alpha_2}}{a_O b_O} \qquad\qquad c_O = \frac{8a_{\beta_o}^3}{a_O b_O} \qquad \textbf{(Eq. 19, 20)}$$

The results for the lattice parameters of the O phase using the data of α_2 and β_o from Tab. 1 are shown in Tab. 5. They are within an acceptable range from the lattice parameters found in Ref. [31] (a=6.09 Å, b=9.57 Å, c=4.67 Å). However, in the case of the O phase the differences between the calculated lattice parameters and the ones found in literature are larger than for the B19 phase. For the O phase the summed absolute deviations amount to 0.65 Å and 0.95 Å, whereas they are between 0.14 Å and 0.35 Å for the B19 phase. One explanation for this is that the O phase is structurally related to the β_o phase, which has different close-packed planes than the α_2 and the γ phase due to its less densely packed crystal structure. Another explanation for the large deviation from the lattice parameters

found in literature is the difference in the chemical compositions of the alloys, in which the lattice parameters were determined. The lattice parameters of the α_2 phase were measured for a Ti-25Al (at.%) alloy and the ones of the β_o phase for a Ti-44Al-2Mo (at.%) alloy [20,21]. However, the lattice parameters of the O phase found in the literature were determined for a Ti-25Al-25Nb (at.%) alloy [31]. Similarly to the B19 phase, using the α_2 lattice parameters produces a smaller deviation from the literature data.

Tab. 5: Calculated lattice parameters of the O phase using the lattice parameters of α_2 and β_o from Tab. 1. The sum of the absolute errors with regard to the lattice parameters in Tab. 4 is shown in the lower part.

		Using the α_2 lattice parameters	Using the β_o lattice parameters
Calculated lattice parameters of the B19 phase [Å]	a	5.765	6.420
	b	9.985	9.079
	c	4.625	4.540
Sum of abs. errors [Å]		0.65	0.95

3.2.2 Alloying systems

For ternary TiAlNb alloys the O phase has been reported in such alloys that contain a significant amount of niobium [32–35]. The O phase exists as an equilibrium phase with the ideal stoichiometry Ti_2AlNb [18]. It was reported firstly by Banerjee et al. [36] in a Ti-25Al-12.5Nb (at.%) alloy, and they assigned a space group to its structure and determined the atomic positions. Muraleedharan et al. [32] investigated the O phase with TEM in the ternary Ti-Al-Nb system with a niobium content up to 25 at.% and a fixed aluminum content of 27.5 at.%. They identified the two different types O1 and O2 and suggested that the transformation from O1 to O2 can be accomplished by a replacive ordering wave. Furthermore, the O phase was found to exhibit a plate-like morphology or mosaic patterns within the microstructure [34]. The phase transformations including the O phase during cooling of ternary TiAlNb alloys near the Ti_2AlNb stoichiometry were investigated by Sadi et al. [35] with scanning differential calorimetry, dilatometry and TEM. During cooling from 1200 °C they observed that the O phase could form via three different reactions, which yielded different microstructures. The transformation of the β_o phase into the O phase led to laths or a needle-like structure. When formed via the transformation of the α_2 phase, the O phase tended to form needles. The last possibility was a peritectoid reaction of the α_2 and the β_o phase, where the O phase appeared at the interface between these two phases. This type of transformation was also found by Muraleedharan et al. [32]. Furthermore, Sadi et al. [35] observed the formation of a massive O phase at high cooling rates from to the β/β_o phase field, which transformed into the equilibrium O phase after an annealing between 700 °C and 900 °C. Popov et al. [37] also investigated an alloy near the ideal Ti_2AlNb

stoichiometry with a chemical composition of Ti-24.3Al-24.8Nb-1.0Zr-1.4V-0.6Mo-0.3Si (at.%). They found that below 750 °C the microstructure consisted of a two phase (β+O) structure. Upon heating a three phase structure consisting of β, α_2 and O phase was formed between 800 °C and 950 °C. At higher temperatures the O phase had dissolved [37]. In literature no evidence has been found that the B19 phase was observed in TiAl alloys with a niobium content of approximately 25 at.%, like in the alloys mentioned above. This shows that the O phase is preferred over the B19 phase for such a type of alloys.

Besides these TiAl alloys near Ti-25Al-25Nb (at.%) the O phase has also been reported in γ-TiAl based alloys, which have a niobium content lower than 25 at.% [7,12,15]. In a recent work Rackel et al. [7] found an orthorhombic phase in a powder metallurgically produced and HIPed γ-TiAl based Ti-42.8Al-8.5Nb (at.%) alloy within a modulated microstructure. Using HEXRD methods they could show that this phase was structurally comparable with the O phase and that it had formed out of the α_2 phase between 500 °C and 700 °C. Furthermore, they observed the dissolution of this orthorhombic phase above 700 °C and that it could be re-precipitated during subsequent slow cooling [7]. This indicates that this orthorhombic phase could be a stable phase. The same alloy was investigated by Gabrisch et al. [12] after annealing at 550 °C and 650 °C. Using single crystal electron diffraction and high-resolution imaging they found the O phase within the α_2 laths of lamellar α_2/γ colonies. They observed O phase domains with a rectangular or rhomboid shape. Also with the help of TEM Ren et al. [15] investigated the O phase in a Ti-45Al-8.5Nb (at.%) alloy. They found that the O phase was part of a modulated microstructure and that it had a thin plate-like shape. Furthermore, they could identify the type of the O phase, which was in this particular case the O1 phase.

Interestingly, for γ-TiAl based alloys of a composition similar to the alloys described above, the B19 phase has also been observed [13,14,28]. This shows the difficulty of the discrimination between the O phase and the B19 phase. However, the appearance of the B19 phase in the γ-TiAl based alloys is in contrast to the ternary TiAlNb alloys with a niobium content of 25 at.%. An explanation could be that due to the lower amount of niobium and a higher amount of aluminum the formation of the B19 phase becomes possible. Another difference between the two types of TiAl alloys is the observed transformation path of the O phase. Rackel et al. [7] found that this phase had formed out of the α_2 phase during cooling of a γ-TiAl based alloy, whereas Muraleedharan et al. [32] reported a peritectiod reaction of α_2 and β_o into the O phase for a ternary TiAlNb alloy.

Martensitic transformations in TiAl alloys

This section deals with the martensitic transformations in γ-TiAl based alloys. However, only the martensitic transformations based on the β/α transformation are dealt with because these are of greater importance for this work than the β/γ transformation.

The β/α transformation is very sensitive to the cooling rate. At low cooling rates Widmanstätten α is formed, which leads to colony or basket-weave microstructures. At higher cooling rates the formation of massive α occurs. Only at very high cooling rates the martensitic transformation takes place [38]. Three different types of martensite can be formed based on the β/α transformation, which are called α', α'' and $α_2$' [39–43]. The face centered orthorhombic α'' martensite is mentioned here only for the sake of completeness, because it tends to form mostly in β titanium alloys [39,44–46]. The α' and the $α_2$' martensite both have a hexagonal crystal structure but the α' is disordered, whereas the $α_2$' martensite is ordered [40].

For binary TiAl alloys the martensitic β/α transformation has never been observed even under ice-brine quenching, probably because of the very high β/α transus-temperature [20,47]. But due to addition of β-stabilizing elements the β/α transus-temperature is shifted to lower temperatures, which might give rise to martensitic transformations [3]. For example, Kastenhuber et al. [41] reported the formation of α' martensite during solidification via gas atomization of a γ-TiAl based Ti-44.1Al-3.9Nb-0.9Mo-0.1B (at.%) alloy, in which the martensite had formed in the aluminum-lean areas during the cooling process. An incomplete martensitic transformation was observed by Hu et al. [48] after an ice-brine quenching in a Ti-44Al-4Nb-4Hf-0.1Si (at.%) alloy, in which the martensite was accompanied by massive $α_2$ plates. The $α_2$' martensite was observed by Chen et al. [42] in a γ-TiAl based Ti-40Al-10V (at.%) alloy. Interestingly, due to the high amount of vanadium and relatively low amount of aluminum the martensitic transformation was achievable even under air cooling conditions. The formation of this type of martensite was also reported by Xu et al. [43] in a Ti-42Al-5Mn (at.%) alloy. However, for this alloy the formation of the martensite only occurred at high cooling rates, which were achieved by water quenching. This shows the dependence of the critical cooling rate, which is needed to form martensite, from the β/α transus-temperature. Because of the lower aluminum content and the presence of the β-

stabilizing element vanadium in the alloy studied by Chen et al. [42], this temperature was lower than in the alloy studied by Xu et al. [43]. Therefore, Chen et al. [42] could observe the martensitic transformation at a lower cooling rate than Xu et al. [43].

Mayer et al. [40] observed the formation of the α_2' martensite in a γ-TiAl based Ti-44.58Al-3.23Mo-0.12B (at.%) alloy, which had basically the same composition as the alloy studied in this work. After water quenching from the β single-phase field a significant amount of α_2' martensite had formed at the expense of the β phase via a local diffusion-controlled transformation together with purely displacive one. The martensite was observed as lath-like structures with a thickness of approximately 0.1 μm [40]. Similarly to Ref. [40], the samples in this work were subjected to a heat treatment in the β single-phase field region and a subsequent water quenching. Thus, it can be expected that the α_2' martensite also occurs in the studied alloy. Indeed, it is found in TEM after water quenching. A TEM image of the α_2' martensite is shown in Fig. 5. The size and the shape of the α_2' martensite are in good agreement with the martensite found by Mayer et al. [40].
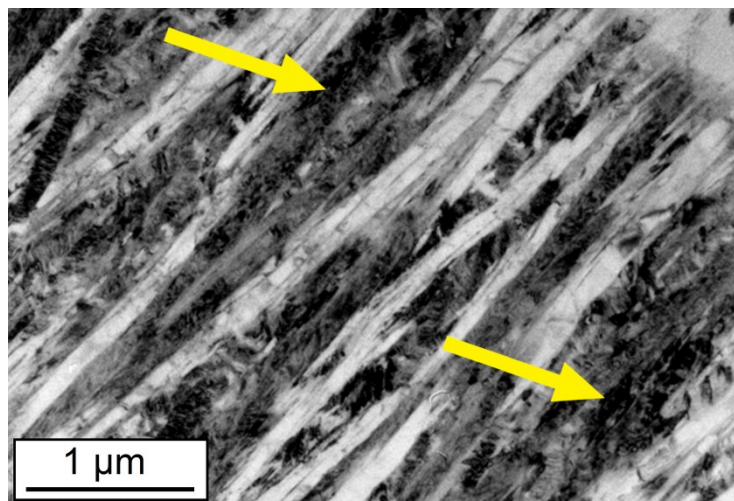
Fig. 5: TEM image of the α_2' martensite found in the studied alloy. Between the light gray martensitic needles the β_o phase can be seen (arrows).

Furthermore, Mayer et al. [49] investigated an alloy with a composition of Ti-43.94Al-6.78Mo-0.09B (at.%). For this alloy, which had a higher molybdenum content than the alloy studied in Ref. [40], no martensitic transformation could be observed during water quenching. A higher amount of β-stabilizing elements decreases the β/α transus-temperature as well as the martensitic start temperature [19]. This suggests that the higher molybdenum content in alloy studied in Ref. [49] had lowered this temperature below room temperature and, thus, no martensitic transformation was observed during water quenching.

_____

Materials and methods

Details about the studied material, the preparation and the experimental parameters can be found in chapter 2 of the appended paper. Here, additional information about the preparation of the SEM and TEM samples, the performed synchrotron experiments and the establishment of the lattice occupancy factors are given.

5.1 Preparation of the SEM and TEM samples

The SEM samples were cut using an ATM precision cutting machine Brilliant 221. One sample was taken from the bulk material after the HIP process and one after the β-homogenization and water-quenching. The SEM samples of the transition state and the end state were taken from the corresponding HEXRD specimens. The SEM samples were embedded in the hot mounting resin Polyfast by Struers with the CitoPress-20 mounting press. A channel of aluminum foil was added to ensure conductivity during the SEM measurements. Afterwards the samples were ground using a TegraPol 5 grinding machine. The parameters of the grinding process can be found in Tab. 6. The grinding machine worked at 300 rpm, and the sample holder and the grinding paper rotated counterclockwise. At last, the samples were polished for 30 seconds with an oxide polishing suspension and cleaned.

Tab. 6: Grinding parameters for the SEM samples.

Grit size	Grinding time [min]	Force/sample [N]
500	3	40
800	4	40
1000	5	25
1200	2 x 5	25
2000	2 x 5	25
4000	2 x 5	25

For the TEM investigations of the water-quenched, the transition and the end state samples with a thickness above 100 μm were cut from corresponding dilatometer specimens. They were ground down to a thickness of 100 μm using a grinding paper with a grit size of 1000, and subsequently pieces with the right size for the TEM sample holder were die-cut out of

them. To achieve a small enough thickness to ensure electron-transparency the samples were electro-polished using the electrolytic polishing system TenuPol-5 and the A3 electrolyte by Struers. A voltage of 25 V, a light stop value of 50 and pump flow rate of 10 were used for the electro-polishing.

5.2 List of the performed synchrotron measurements

Table 7 shows a list of all synchrotron measurements, which were performed as part of this work in August and November 2018 at the Deutsches Elektronen Synchrotron (DESY).

Tab. 7: Short designations of the synchrotron measurements with the measurement date, the mean beam energy and a short description of the temperature/time evolution during each measurement.

Name	Date	Energy [keV]	Temperature / Time
TiAl1	Aug. 2018	100	Heating from 400 °C to 900 °C at 2 K/min
TiAl2	Aug. 2018	100	Ageing at 600 °C for 8 h
TiAl8	Aug. 2018	100	Heating to 1450 °C at 200 K/min and quenching at 200 K/s
TiAl11	Aug. 2018	100	Ageing at 700 °C for 2 h
TiAl12	Aug. 2018	100	Heating from 500 °C to 800 °C to 500 °C at 2 K/min
TiAl15	Nov. 2018	87.1	Ageing at 650 °C for 2 h
TiAl16	Nov. 2018	87.1	Heating from 575 °C to 720 °C to 575 °C at 0.5 K/min

5.3 Establishment of the site occupancy factors

In order to establish the site occupancy factors for each phase the results of the EDX measurements were used, which can be found in chapter 3.2 of the appended paper. In combination with the findings of Holec et al. [24] the initial values for the occupancy factors were derived. Molybdenum was placed on its preferred sublattice and titanium and aluminum were distributed on the corresponding sublattices. To account for the non-stoichiometric phase composition due to the water quenching, some of the titanium and aluminum was placed on the other sublattice in such a way that the phase composition matched the EDX results. For example, the composition of the α_2 phase after the water quenching is 54.6Ti-42.4Al-3.0Mo (at.%). In this phase the molybdenum occupies the Ti sublattice and, therefore, all of this element was placed on this lattice, which yielded 4 at.%. Distributing the titanium and aluminum yielded for the Ti sublattice 65Ti-31Al-4Mo (at.%) and for the Al sublattice 24Ti-76Al-0Mo (at.%) as initial values. These were inserted into the phase models created in the software program MAUD. For each phase the fractions of the elements were changed by hand until the best possible fit was obtained, which yielded the adjusted site occupancy factors. These are shown in Tab. 1 in the appended paper. For the example of the α_2 phase they accounted to 69.5Ti-26.5Al-4.0Mo (at.%) for the Ti sublattice and 10.0Ti-90.0Al-0.0Mo (at.%) for the Al sublattice.

_____

Results and discussion

The major results and discussion can be found in chapter 3 in the paper in the appendix. There the three ex situ states, called the "water-quenched state", the "transition state" and the "end state" are described in detail regarding their microstructures and diffractograms. Furthermore, the characterization of the orthorhombic phase and the main results of the Rietveld refinement of the diffraction data are shown. Additionally, the performed _in situ_ synchrotron experiments as well as the results of the TEM investigations of the three states are described. This section offers additional information about the topic. The first subchapter deals with the peak splitting of the α_2 phase during the _in situ_ measurements. Diffractograms at various temperatures are shown, which should give a clear impression about the change in the diffraction data. The second subchapter describes the evolution of the phase fractions during an _in situ_ heating and an _in situ_ annealing experiment.

6.1 The peak splitting due to the orthorhombic phase

Figure 6a shows the evolution of the azimuthally integrated intensities as a function of temperature for an _in situ_ heating experiment from 400 °C to 900 °C at 2 K/min. At temperatures below 600 °C, which corresponds to the water-quenched state, only the α_2 and the β_o phase are present. When exceeding 600 °C the transition state is formed within the specimen, which is characterized by the formation of the orthorhombic phase. In order to illustrate the peaks of this phase, the peak positions of the B19 phase are shown. A good example illustrating this fact is the α_2-(110) peak at a Bragg angle of 2.45°. The corresponding B19 peak is located at a slightly lower Bragg angle, which leads to a shift of the peak towards smaller Bragg angles during the formation of the orthorhombic phase. Furthermore, in Fig. 6a the γ formation becomes obvious at temperatures above 700 °C, which yields the end state. The γ-(001) and the γ-(002)/(200) peaks indicate that the formation of this phase coincides with the dissolution of the orthorhombic phase and that a large amount of γ is formed in a rather small temperature interval. As mentioned in the appended paper in chapter 3.2 the molybdenum partitions to the β_o phase, which lowers its superstructure reflections in terms of maximum intensity. In Fig. 6a the continuous decrease

of the superstructure reflections with increasing temperature can be seen at the example of the β_o-(100) peak.

The splitting of the α_2-(200) peak as a function of temperature during an *in situ* heating experiment is shown in Fig. 6b. At temperatures below 600 °C only the α_2 peak is visible. When exceeding this temperature, the α_2 peak begins to split due to the increasing amount of the orthorhombic phase, which has two separate peaks in this Bragg angle region. After the maximum peak separation at approximately 650 °C the splitting continuously decreases until at 724 °C the orthorhombic phase has completely vanished and only the α_2-(200) peak is visible.

Fig. 6: (a) shows the azimuthally integrated intensities as a function of time during an *in situ* heating experiment; (b) shows the splitting of the α_2-(200) peak between 600 °C and 750 °C (arrows).

6.2 Evolution of the phase fractions

The evolution of the phase fractions during an *in situ* heating experiment from 400 °C to 900 °C is shown in Fig. 7a. The phase fractions were evaluated at certain temperatures with Rietveld refinement of the diffraction data. For the Rietveld analysis of the synchrotron diffraction data the structure of the B19 phase was used to describe the orthorhombic phase. At 400 °C the sample consists of approximately 84 vol.% α_2 and 16 vol.% β_o phase. The amount of β_o phase only shows minor changes during the experiment, which range between 10 vol.% and 16 vol.%. During further heating the amount of α_2 phase slightly increases, whereas the β_o phase fraction decreases. When approaching 600 °C the orthorhombic phase is formed. The formation starts at 590 °C. However, due to the large overlap of the α_2 peaks and the peaks of the orthorhombic phase a reasonable evaluation of the phase fractions is only possible for a sufficient amount of B19 phase. At 650 °C the orthorhombic phase reaches its maximum phase fraction of 55 vol.% and then decreases up to a temperature of 724 °C. When the orthorhombic phase is formed, the amount of α_2

decreases from 88 vol.% to 40 vol.%. During the dissolution of the orthorhombic phase, however, it remains constant. This in combination with the formation of the γ phase during the dissolution of the orthorhombic phase clearly shows the role of the orthorhombic phase as a transition phase between the α_2 and the γ phase. After the orthorhombic phase has completely vanished, the amount of α_2 decreases further, whereas the γ phase fraction increases, as the system approaches a near equilibrium condition.

Figure 7b shows the evolution of the phase fractions during an *in situ* isothermal ageing treatment at 700 °C as a function of time. Shortly after reaching the ageing temperature the orthorhombic phase fraction approaches its maximum of 52 vol.%, which is only slightly lower than in the heating experiment. The formation and dissolution of the phases is qualitatively the same as described above. Two additional things should be mentioned. Firstly, there is a drop of about 10 vol.% in the β_o phase fraction at the beginning, partly in favor of a slightly increasing α_2 phase fraction. And secondly, the retained amount of α_2 phase is larger than the one after the heating experiment. The reason for this might be that the ageing temperature is 700 °C, whereas during the heating experiment the maximum temperature reached is 900 °C.
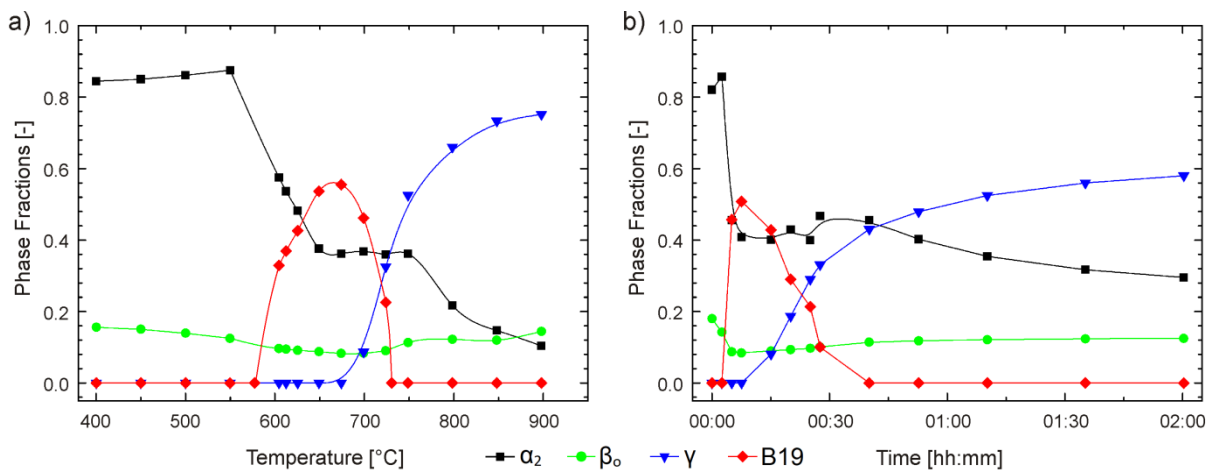
Fig. 7: Evolution of the phase fraction for (a) an *in situ* heating experiment from 400 °C to 900 °C at 2 K/min and (b) an *in situ* ageing experiment at 700 °C for 2 hours.

Conclusions

The aim of this work was to identify the type of the orthorhombic phase formed during the reheating of a water-quenched Ti-44.5Al-3.2Mo-0.1B (at.%) alloy. Furthermore, the temperature interval of its formation and dissolution as well as its phase stability should be investigated. For the characterization of this orthorhombic phase *in situ* high-energy synchrotron X-ray diffraction combined with Rietveld analysis was used. With the help of scanning and transmission electron microscopy the evolution of the microstructure was studied.

The diffraction data show that after the water quenching from the β single-phase field region the samples consist of approximately 85 vol.% α_2 phase and 15 vol.% β_o phase. During the heating experiments a splitting of the α_2 peaks in the diffraction data occurs, which can be attributed to the formation of an orthorhombic phase. This formation starts at 590 °C and at a temperature of approximately 650 °C its maximum phase fraction of 55 vol.% is reached. This large increase in its phase fraction, however, leads to a significant decrease in the α_2 phase fraction to about 40 vol.%. Further heating yields the dissolution of the orthorhombic phase, until at 724 °C it has vanished completely. Its dissolution coincides with the formation of the γ phase, from which can be concluded that this orthorhombic phase acts as a transition phase between the α_2 and the γ phase. After the orthorhombic phase has vanished a further decrease in the α_2 phase fraction is observed and, simultaneously, the amount of γ phase increases. Finally this leads to a near equilibrium state with a large amount of γ and retained α_2 and β_o phase.

For γ-TiAl based alloys two orthorhombic phases are reported in the literature, called B19 phase and O phase [7,8,12,14]. It is not possible to identify the type of the orthorhombic phase with the performed investigations. However, with a Rietveld analysis of the diffraction data, the formed orthorhombic phase is characterized regarding its lattice parameters, formation and dissolution temperatures and phase fraction. The lattice parameters of the B19 phase were evaluated using Rietveld refinement. For the investigated alloy, they amount to a=4.615 Å, b=2.920 Å, c=4.889 Å, which is in a good agreement with literature [8,25]. Also the temperature interval between 590 °C and 724 °C for the formation of the orthorhombic phase is similar to the one found in literature [7,8]. With increasing heating

rate during the *in situ* experiments the temperature interval, in which the orthorhombic phase is present, is shifted to higher temperatures. Furthermore, all performed synchrotron experiments show consistent results. With the help of an *in situ* heating and cooling experiment it is shown that this phase is metastable in the investigated alloy. It only forms upon reheating after water quenching. When a cooling is conducted after the orthorhombic phase has vanished and the γ phase is present, no further formation of the orthorhombic phase is observable.

After water quenching the SEM reveals a microstructure, which consists of large α_2 laths with a mixture of fine phases in between. TEM investigations have shown that this phase mixture is essentially α_2' martensite and β_o phase, which have formed so small structures that they cannot be resolved in SEM at the given magnification. The formation of the orthorhombic phase upon reheating leads to the formation of a so-called modulated microstructure, in which the orthorhombic phase is present in form of fine lamellae within the α_2 laths and the α_2' martensite. The name "modulated microstructure" stems from the modulation of the contrast inside the lamellae when investigated by means of TEM. The TEM investigations reveal that the γ phase, which forms during the dissolution of the orthorhombic phase, is present within the α_2 laths as well as the α_2' martensite. The γ phase has also formed lamellae similar to the orthorhombic phase. So in the near equilibrium state the microstructure consists of large α_2 laths with small γ lamellae within. Between these laths a mixture of α_2' martensite with γ lamellae and β_o phase is present. This specific change in the microstructure could only be observed with TEM, while in the SEM no difference can be spotted between the single states.

References

[1]   H. Kestler, H. Clemens, Production, processing and application of γ(TiAl)-based alloys, in: M. Peters, C. Leyens (Eds.), Titanium and titanium alloys: Fundamentals and applications, Wiley-VCH Verlag, Weinheim, 2003: pp. 351–393.

[2]   H. Clemens, S. Mayer, Intermetallic titanium aluminides as innovative high temperature lightweight structural materials-How materialographic methods have contributed to their development, Pr. Met. 52 (2015) 691–721.

[3]   H. Clemens, S. Mayer, Design, processing, microstructure, properties, and applications of advanced intermetallic TiAl alloys, Adv. Eng. Mater. 15 (2013) 191–215.

[4]   F. Appel, M. Oehring, γ-titanium aluminide alloys: alloy design and properties, in: M. Peters, C. Leyens (Eds.), Titanium and titanium alloys: Fundamentals and applications, Wiley-VCH Verlag, Weinheim, 2003: pp. 89–152.

[6]   A. Stark, M. Oehring, F. Pyczak, A. Schreyer, In situ observation of various phase transformation paths in Nb-rich TiAl alloys during quenching with different rates, Adv. Eng. Mater. 13 (2011) 700–704.

[7]   M.W. Rackel, A. Stark, H. Gabrisch, N. Schell, A. Schreyer, F. Pyczak, Orthorhombic phase formation in a Nb-rich γ-TiAl based alloy – An in situ synchrotron radiation investigation, Acta Mater. 121 (2016) 343–351.

[8]   T. Schmoelzer, A. Stark, E. Schwaighofer, T. Lippmann, S. Mayer, H. Clemens, In situ synchrotron study of B19 phase formation in an intermetallic γ-TiAl Alloy, Adv. Eng. Mater. 14 (2012) 445–448.

[9]   H. Clemens, S. Mayer, Intermetallic γ-titanium aluminide based alloys from a metallographic point of view – a continuation, Pr. Met. 48 (2011) 64–100.

[10]   T. Schmoelzer, S. Mayer, C. Sailer, F. Haupt, V. Güther, P. Staron, K.D. Liss, H. Clemens, In situ diffraction experiments for the investigation of phase fractions and ordering temperatures in Ti-44 at% Al-(3-7) at% Mo alloys, Adv. Eng. Mater. 13 (2011) 306–311.

[11]   T. Klein, H. Clemens, S. Mayer, Advancement of compositional and microstructural design of intermetallic γ-TiAl based alloys determined by atom probe tomography, Materials (Basel) 9 (2016) 1–19.

[12]   H. Gabrisch, U. Lorenz, F. Pyczak, M. Rackel, A. Stark, Morphology and stability of orthorhombic and hexagonal phases in a lamellar γ-Ti-42Al-8.5Nb alloy - A transmission electron microscopy study, Acta Mater. 135 (2017) 304–313.

[13] F. Appel, J.D.H. Paul, M. Oehring, Phase transformations during creep of a multiphase TiAl-based alloy with a modulated microstructure, Mater. Sci. Eng. A 510–511 (2009) 342–349.

[14] L. Song, X.J. Xu, L. You, Y.F. Liang, J.P. Lin, B19 phase in Ti–45Al–8.5Nb–0.2W–0.2B–0.02Y alloy, J. Alloys Compd. 618 (2015) 305–310.

[15] G. dong Ren, J. Sun, High-resolution electron microscopy characterization of modulated structure in high Nb-containing lamellar γ-TiAl alloy, Acta Mater. 144 (2018) 516–523.

[16] I. Ohnuma, Y. Fujita, H. Mitsui, K. Ishikawa, R. Kainuma, K. Ishida, Phase equilibria in the Ti-Al binary system, Acta Mater. 48 (2000) 3113–3123.

[17] L. Usategui, M.L. Nó, S. Mayer, H. Clemens, J. San Juan, Internal friction and atomic relaxation processes in an intermetallic Mo-rich Ti-44Al-7Mo ($\gamma+\beta_o$) model alloy, Mater. Sci. Eng. A 700 (2017) 495–502. doi:10.1016/j.msea.2017.06.014.

[18] A. Stark, Textur- und Gefügeentwicklung bei der thermomechanischen Umformung Nb-reicher γ-TiAl-Basislegierungen, PhD. Thesis, Shaker Verlag, Aachen, 2010.

[19] M. Peters, J. Hemptenmacher, J. Kumpfert, C. Leyens, Structure and properties of titanium and titanium alloys, in M. Peters, C. Leyens (Eds.), Titanium and titanium alloys: Fundamentals and applications, Wiley-VCH Verlag, Weinheim, 2003: pp. 1–36.

[20] F. Appel, J.D.H. Paul, M. Oehring, Gamma titanium aluminide alloys: science and technology, Wiley-VCH Verlag, Weinheim, 2011: pp. 9-10

[21] Y.G. Li, M.H. Loretto, Microstructure and fracture behaviour of Ti-44Al-xM derivatives, Acta Metall. 42 (1994) 2913–2919.

[22] Y.-W. Kim, Intermetallic alloys based on gamma titanium aluminide, J. Miner. Met. Mater. Soc. 41 (1989) 24–30.

[23] M. Blackburn, Some aspects of phase transformation in titanium alloys, in: R.I. Jaffee, N.E. Promisel (Eds.), The science, technology and application of titanium, Oxford Pergamon Press Ltd., 1970: pp. 633–643.

[24] D. Holec, R.K. Reddy, T. Klein, H. Clemens, Preferential site occupancy of alloying elements in TiAl-based phases, J. Appl. Phys. 119 (2016) 1–8.

[25] E. Abe, T. Kumagai, M. Nakamura, New ordered structure of TiAl studied by high-resolution electron microscopy, Intermetallics 4 (1996) 327–333.

[26] M. Tanimura, Y. Inoue, Change in Al concentration profile related to the $D0_{19} \rightarrow L1_0$ structural change in Ti-Al alloys, Scr. Mater. 44 (2001) 365–373.

[27] F. Appel, M. Oehring, J.D.H. Paul, Nano-scale design of TiAl alloys based on β-phase decomposition, Adv. Eng. Mater. 8 (2006) 371–376.

[28] F. Appel, M. Oehring, J.D.H. Paul, A novel in situ composite structure in TiAl alloys, Mater. Sci. Eng. A 493 (2008) 232–236.

[29]   D. Nguyen-Manh, D.G. Pettifor, Origin of O phase and pseudo-twinning in Ti-Al-Nb alloys: A first-principles study, Y.-W. Kim, D.M. Dimiduk,M.H. Loretto (Eds.), Gamma titanium aluminides, TMS, Warrendale, PA, 1999, p. 175.

[30]   R. Ducher, B. Viguier, J. Lacaze, Modification of the crystallographic structure of γ-TiAl alloyed with iron, Scr. Mater. 47 (2002) 307–313.

[31]   B. Mozer, A. Bendersky, W.J. Boettinger, Neutron powder diffraction study of the orthorhombic Ti_2AlNb phase, Scr. Metall. Mater. 24 (1990) 2363-2368.

[32]   K. Muraleedharan, T.K. Nandy, D. Banerjee, S. Lele, Phase stability and ordering behaviour of the O phase in TiAlNb alloys, Intermetallics 3 (1995) 187–199.

[33]   D. Banerjee, The intermetallic Ti_2AlNb, Prog. Mater. Sci. 42 (1997) 135–158.

[34]   K. Muraleedharan, D. Banerjee, Phase transformations involving the α_2 and O phases in Ti-Al-Nb alloys, Scr. Metall. Mater. 9 (1993) 527–532.

[35]   F.A. Sadi, C. Servant, On the B2→O phase transformation in Ti–Al–Nb alloys, Mater. Sci. Eng. A 346 (2003) 19–28.

[36]   D. Banerjee, A.K. Gogia, T.K. Nandy, V.A. Joshi, A new ordered orthorhombic phase in a Ti_3Al-Nb alloy, Acta Metall. 36 (1988) 871–882.

[37]   A.A. Popov, A.G. Illarionov, S. V. Grib, S.L. Demakov, M.S. Karabanalov, O.A. Elkina, Phase and structural transformations in the alloy on the basis of the orthorhombic titanium aluminide, Phys. Met. Metallogr. 106 (2008) 399–410.

[38]   T. Ahmed, H.J. Rack, Phase transformations during cooling in α+β titanium alloys, Mater. Sci. Eng. A 243 (1998) 206–211.

[39]   M. Grujicic, P. Dang, Martensitic transformation in a dispersed Ti-Al-V-Fe β-phase and its effect on fracture toughness of γ-titanium aluminide, Mater. Sci. Eng. A 224 (1997) 187–199.

[40]   S. Mayer, M. Petersmann, F.D. Fischer, H. Clemens, T. Waitz, T. Antretter, Experimental and theoretical evidence of displacive martensite in an intermetallic Mo-containing γ-TiAl based alloy, Acta Mater. 115 (2016) 242–249.

[41]   M. Kastenhuber, T. Klein, B. Rashkova, I. Weißensteiner, H. Clemens, S. Mayer, Phase transformations in a β-solidifying γ-TiAl based alloy during rapid solidification, Intermetallics 91 (2017) 100–109.

[42]   Y. Chen, L. Cheng, L. Sun, Y. Lu, G. Yang, H. Kou, E. Bouzy, Characterization of a new microstructure in a β-solidifying TiAl alloy after air-cooling from a β phase field and subsequent tempering, Metals (Basel) 8 (2018) 1–11.

[43]   H. Xu, X. Li, W. Xing, L. Shu, Y. Ma, K. Liu, Intermetallics phase transformation behavior of a Mn containing β-solidifying γ-TiAl alloy during continuous cooling, Intermetallics 99 (2018) 51–58.

[44]   E. Aeby-Gautier, A. Settefrati, F. Bruneseaux, B. Appolaire, B. Denand, M. Dehmas, G. Geandier, P. Boulet, Isothermal α″ formation in β metastable titanium alloys, J. Alloys Compd. 577 (2013) S439–S443.

[45]   S. Sadeghpour, S.M. Abbasi, M. Morakabati, Deformation-induced martensitic transformation in a new metastable β titanium alloy, J. Alloys Compd. 650 (2015) 22–29.

[46]   P. Barriobero-Vila, V. Biancardi Oliveira, S. Schwarz, T. Buslaps, G. Requena, Tracking the α″ martensite decomposition during continuous heating of a Ti-6Al-6V-2Sn alloy, Acta Mater. 135 (2017) 132–143.

[47]   Y. Yamabe, M. Takeyama, M. Kikuchi, Microstructure evolution through solid-solid phase transformations in gamma titanium aluminides, in: Y.W. Kim, R. Wagner, M. Yamaguchi (Eds.), Gamma Titanium Aluminides, TMS, Warrendale, PA, 1995: pp. 111–129.

[48]   D. Hu, H. Jiang, Martensite in a TiAl alloy quenched from beta phase field, Intermetallics 56 (2015) 87–95.

[49]   S. Mayer, C. Sailer, T. Schmoelzer, H. Clemens, T. Lippmann, P. Staron, V. Güther, M. Takeyama, On phase equilibria and phase transformations in β/γ-TiAl alloys – A short review, BHM Berg- und Hüttenmännische Monatshefte 156 (2011) 438–442.

_____

Appendix

Evidence of an orthorhombic transition phase in a Ti-44Al-3Mo (at.%) alloy using *in situ* synchrotron diffraction and transmission electron microscopy

Michael Musi [a], Petra Erdely [b], Boryana Rashkova [a], Helmut Clemens [a], Andreas Stark [c], Peter Staron [c], Norbert Schell [c], Svea Mayer [a,*]

[a] Department of Physical Metallurgy and Materials Testing, Montanuniversität Leoben, Roseggerstr. 12, 8700 Leoben, Austria; michael.musi@unileoben.ac.at, helmut.clemens@unileoben.ac.at, boryana.rashkova@unileoben.ac.at

[b] Recipient of a DOC Fellowship of the Austrian Academy of Science at the Department of Physical Metallurgy and Materials Testing, Montanuniversität Leoben, Roseggerstr. 12, 8700 Leoben, Austria; petra.erdely@unileoben.ac.at

[c] Institute of Materials Research, Helmholtz-Zentrum Geesthacht, Max-Planck-Str. 1, 21502 Geesthacht, Germany; andreas.stark@hzg.de, peter.staron@hzg.de, norbert.schell@hzg.de

[*] Corresponding author. Tel.: +43 3842 402 4210; fax: +43 3842 402 4202
E-mail address: svea.mayer@unileoben.ac.at (Svea Mayer).

Abstract

Alloying of a binary system with an additional element often leads to the formation of new phases. In this work, a γ-TiAl based alloy with 3 at.% molybdenum was investigated, which was quenched from 1450 °C. Upon reheating, the formation of an orthorhombic phase was observed with the help of *in situ* high-energy X-ray diffraction. This phase formed at 600 °C and vanished at 720 °C, and acts as a transition phase between the α_2 and the γ phase. Such a transition phase has not been observed before in this type of alloy. Additionally, transmission electron microscopy was used to study the microstructure of selected sample states on a sub-micrometer level. The orthorhombic phase formed fine lamellae inside the α_2 phase and the α_2' martensite.

Highlights:

- In water-quenched Ti-44Al-3Mo (at.%) an orthorhombic phase is formed upon reheating
- The orthorhombic phase is identified as a metastable phase
- It acts as transition phase between α_2 and γ between 600 °C and 720 °C
- It forms a modulated microstructure within the α_2 phase and the α_2' martensite

Keywords:

Titanium aluminides, Orthorhombic phase, High-energy X-ray diffraction, Transmission electron microscopy, *In situ*, Transition phase

1. Introduction

Due to their outstanding properties, such as a low density, high specific stiffness, high specific strength, and good creep resistance, TiAl alloys are well suited for applications in the aerospace and automotive industry [1]. For example, a γ-TiAl based alloy, the so-called TNM alloy, is already used as turbine blade material in an eco-friendly aeroengine [2]. Besides aluminum, the alloying elements niobium and molybdenum - hence the designation TNM - contribute to the excellent properties of this alloy [2]. The addition of these elements, however, influences the existing phases and can lead to the formation of new phases. Therefore, it is mandatory for the application to understand which phases can occur under certain conditions. This paper deals with the formation of an orthorhombic phase in a Ti-44.5Al-3.2Mo-0.1B (at.%) model alloy during reheating after quenching from the β single-phase field region using *in situ* synchrotron X-ray diffraction and transmission electron microscopy.

Under thermodynamic equilibrium conditions, various phases can occur in an alloy of the chemical composition studied in this work. Upon cooling from the liquid single-phase field region, the disordered bcc β-Ti(Al) phase (A2 structure, Im-3m) forms. During further cooling, a part of the β phase transforms into the disordered hexagonal α-Ti(Al) phase (A3, P63/mmc). Thereafter, the tetragonal γ-TiAl phase (L1$_0$, P4/mmm) is precipitated. Additionally, the α and β phase show an order transformation into the ordered hexagonal α$_2$-Ti$_3$Al (D0$_{19}$, P63/mmc) and the ordered β$_o$-TiAl (B2, Pm-3m) phase. At ambient temperatures the α$_2$, the β$_o$ and the γ phase coexist [3,4]. So in comparison to the binary Ti-Al system, the β$_o$ phase is stabilized at room temperature due to the addition of the β-stabilizing element molybdenum. Another often used β-stabilizing element is niobium [3,5].

When a sufficient amount of these two elements, i.e. niobium and/or molybdenum, is added to the Ti-Al system, the formation of stable or metastable orthorhombic phases is possible [6–11]. In recent years, a growing body of literature is devoted to on the O phase (A$_2$BC, Cmcm), which was observed first by Banerjee et al. [6] in ternary Ti-25Al-12.5Nb (at.%). Muraleedharan et al. [7] investigated the formation and the morphology of the O phase in the Ti-27.5Al-(0-25)Nb (at.%)

system and found two different types of the O phase, which they called O1 and O2. These O1 and O2 phases differed in the occupation of the Wyckoff positions 4c1 and 4c2. With the help of *in situ* high-energy X-ray diffraction (HEXRD) Rackel et al. [12] recently observed an orthorhombic phase in a γ-TiAl based Ti-42Al-8.5Nb (at.%) alloy produced via powder metallurgy. The orthorhombic phase was stable in a temperature range from 550 °C to 700 °C and originated from the α_2 phase. Furthermore, they could show that this phase corresponded structurally to the O phase and formed within a tweed-like substructure of a modulated microstructure. Gabrisch et al. [13], who investigated an alloy of the same chemical composition as in Ref. [12], examined the O phase after annealing. Using single crystal electron diffraction and high-resolution imaging they discovered O phase domains with a rectangular or rhomboid shape. In a recent work, Ren et al. [14] observed the O phase in a Ti-45Al-8.5Nb (at.%) alloy. It had formed with a thin plate-like morphology within a modulated microstructure. Additionally, Ren et al. [14] were able to determine the type of the O phase, which was in this particular case the O1 phase.

The second orthorhombic phase reported frequently in literature is the B19 phase (B19, Pmma). Appel et al. [15–17] reported on the formation of this phase in a Ti-(40-44)Al-8.5Nb (at.%) alloy. Using high-resolution transmission electron microscopy they identified the B19 phase within a modulated structure in a lamellar microstructure. Furthermore, they suggested that it was formed via decomposition of the β_o phase. Song et al. [18] observed the B19 phase in a Ti-45Al-8.5Nb-0.2W-0.2B-0.02Y (at.%) alloy and found that it was stable below 900 °C. Interestingly, in this alloy the B19 phase had formed a modulated structure within the α_2 phase, which is in contrast to the formation suggested by Appel et al. [17]. During an *in situ* HEXRD heating experiment of a β-homogenized and water-quenched Ti-45Al-3Mo-0.1B (at.%) alloy Schmoelzer et al. [11] observed a splitting of the α_2 peaks. They suggested that this splitting was due to the formation of the B19 phase. The temperatures, at which this phase occurred, ranged from 600 °C to 700 °C [11].

In sum, literature suggests that the chemical composition of the alloy as well as the experienced thermal history have a major influence on the type of the orthorhombic phase as well as

the transformation path. Additionally, the discrimination between the B19 and the O phase is a delicate issue. From a crystallographic point of view both phases only differ in the occupation of their sublattices. In the B19 phase the Wyckoff positions 4c1 and 4c2 show the same occupation, whereas in the O phase it differs for both sites [12]. While previous work has focused strongly on high Nb-containing γ-TiAl based alloys [12,13,15–17], further evidence is critically needed concerning orthorhombic phases in Mo-containing alloy variants. In particular, characterizaton of the orthorhombic phase formed in these γ-TiAl based alloys is still lacking. The present work provides this missing link in a detailed study of the formation and dissolution of the orthorhombic phase upon reheating of a Ti-44.5Al-3.2Mo-0.1B (at.%) alloy after a β-homogenization treatment and water quenching. *In situ* HEXRD at a synchrotron radiation source combined with Rietveld analysis was used to characterize the orthorhombic phase and to study if it is a stable or metastable phase. Its role as transition phase between α_2 and γ was also investigated. Additionally, the lattice parameters and the site occupancy factors of titanium, aluminum and molybdenum in the different occurring phases were evaluated. Scanning electron microscopy (SEM) and transmission electron microscopy (TEM) were carried out on different annealed samples to monitor the change of the microstructure due to the formation of the orthorhombic phase.

2. Material and Methods

The alloy studied in this paper was produced by GfE Metalle und Materialien GmbH, Nuremberg, Germany, via centrifugal casting and had a chemical composition of Ti-44.5Al-3.2Mo-0.1B (at.%). Boron was added to refine the microstructure upon casting due to formation of borides already in the melt. To close the casting porosity and minimize segregations, a hot isostatic pressing (HIP) was conducted at 1200 °C for 240 min at a maximum pressure of 200 MPa, followed by furnace cooling. Cylindrical samples with an approximate diameter of 4 mm and a length of 7 mm were cut from the bulk material. These were subjected to a β-homogenization treatment at 1450 °C for 30 minutes and a subsequent water quenching. This water-quenched state was the initial state for the synchrotron

radiation experiments.

The synchrotron radiation measurements were performed at the HZG-run P07 beamline at PETRA III at the Deutsches Elektronen Synchrotron (DESY), Hamburg, Germany. The specimens were measured in transmission with a beam cross-section of 1 x 1 mm^2. The mean energy of the synchrotron radiation beam throughout the measurements was 100 keV, which correspond to wavelength of 0.1240 Å. For the *in situ* heating and ageing experiments a modified DIL 805A/D dilatometer (TA Instruments) was used, in which the samples were heated via an induction coil and cooled via argon gas [19]. A thermocouple was spot-welded directly onto the samples to measure the temperature. A Perkin Elmer XRD 1621 flat panel detector at a distance of approximately 1600 mm from the sample was used to record the Deby-Scherer diffraction rings. To determine the exact sample-to-detector distance and the instrumental parameters a lanthanum hexaboride powder sample was inserted into the synchrotron radiation beam. The heating and cooling experiments were performed in a temperature range of 400 °C to 900 °C with constant heating/cooling rates of 0.5 or 2 K/min. During the isothermal ageing experiments the samples were heated at 400 K/min and subsequently held either at 600 °C for 8 hours, at 650 °C for 2 hours or at 700 °C for 2 hours. For the integration of the diffraction patterns and the calibration the software program Fit2D was used [20]. The Rietveld analysis of the integrated diffraction data to evaluate the phase fractions and lattice parameters of the different phases was performed with the software program MAUD [21].

Samples for SEM and TEM investigations were cut either from the precursor material or from the isothermally annealed HEXRD specimens. Four different sample states were prepared. For the "HIPed state" a sample was taken from the material after the HIP process. The "water-quenched state" corresponds to a sample after a β-homogenization treatment at 1450 °C for 30 minutes and subsequent water quenching. A sample state, in which the orthorhombic phase was present, was produced via an annealing treatment of a water-quenched sample at 600 °C for 8 hours. In the following this sample state is called "transition state". With the heating of a water-quenched sample to 900 °C at 2 K/min a sample state was reached, in which the B19 phase had vanished and the γ

phase had formed. This state is referred to as "end state". The SEM images were taken on a Zeiss EVO50 in backscattered electron (BSE) mode at an acceleration voltage of 15 kV. The TEM samples were ground down to a thickness of 100 μm and subsequently electro-polished. The TEM investigations were performed on a Philips CM 12 with an acceleration voltage of 120 kV and a TECNAI F20 with an acceleration voltage of 200 kV. The energy-dispersive X-ray spectroscopy (EDX) measurements were conducted at the Philips CM 12 with an EDAX system.

3. Results and Discussion

3.1. Overall microstructure and diffraction patterns of four selected sample states

The initial state for the synchrotron radiation measurements, the water-quenched state, was produced from the HIPed samples via a β-homogenization treatment at 1450 °C for 30 minutes and subsequent water quenching. Due to the fast quenching the microstructure and the occurring phases are far from the thermodynamic equilibrium. When comparing with a near-equilibrium state, as obtained e.g. after the HIP process, large differences in the microstructure as well as in the diffraction pattern can be observed. In the center of Fig. 1 the characteristic room temperature diffraction patterns of the four different sample states are shown. Next to these, SEM images of the corresponding microstructures are located. From the diffraction pattern of the HIPed state (Fig. 1a) it is visible that the phases α_2, β_o and γ are present. In the water-quenched state (Fig. 1b), however, only the α_2 and the β_o phase exist. The formation of γ is suppressed due to the high cooling rate. The microstructure in this state mainly consists of large α_2 laths or needles, which exhibit a dark contrast in the BSE mode. Between these, a brighter-looking phase is present. TEM investigations have shown, however, that this second phase is indeed a mixture of β_o phase and α_2' martensite, as was reported by Mayer et al. [4] for this kind of alloy. A detailed description of the microstructure on the sub-micrometer level will be given in chapter 3.3. In contrast to these needle-like structures, lamellar α_2/γ colonies are present in the HIPed state, which contain fine β_o precipitates. The colonies of this state are furthermore surrounded by a mixture of β_o and globular γ [2].

Upon heating, the diffraction rings change. When comparing the water-quenched state with the transition state (Fig. 1c) that forms upon annealing at 600 °C for 8 hours and cooling to room temperature, one can observe a splitting of α_2 peaks. A good example is the α_2-(20$\bar{2}$0) peak, which has split into two separate rings. This splitting of the α_2 peaks is attributed to the formation of an orthorhombic phase [11,12]. When comparing the SEM images of the water-quenched state and this transition state no differences can be seen at this level of magnification. However, the diffraction data suggest the formation of an orthorhombic phase. So this phase must have formed very fine structures within the microstructure, whereas the main microstructural components, such as the α_2 laths, have not changed in size or shape.

In Fig. 1d the SEM image and the corresponding diffraction pattern at room temperature are shown for the end state. The orthorhombic phase has vanished and a significant amount of γ phase has formed. For example, the occurrence of the γ-(002)/(200) double peak is a good indicator for this. It should be noted that for this experimental setup γ-(002) and γ-(200) strongly overlap and appear as one peak. Although the formation of γ is clearly visible in the diffraction pattern, again no difference can be observed in the SEM images of the microstructure when comparing the end state with the previous ones at the given magnification in Fig 1. The needle- or lath-like structures with a mixture of phases in between are still present. Thus, the formed γ phase has to be fine-grained, because it cannot be resolved in the micrograph shown in Fig. 1. It can be concluded that the temperature of 700 °C was too low during the experiments and the holding time of 2 hours was too short to induce a change in the appearance of the overall microstructure, while phase transformations must have taken place at the sub-micrometer level.

Figure 2 shows the azimuthally integrated diffraction data to illustrate the differences between the water-quenched state (Fig. 2a), the transition state (Fig. 2b) and the end state (Fig. 2c). At the top the positions of the reflections of the individual phases are indicated. The peak positions the orthorhombic phase were indexed according to the B19 structure. In the water-quenched state it can now clearly be seen that no γ phase is present, and the α_2 phase has the highest phase fraction.

The remaining fraction is β_o phase. When exceeding approximately 600 °C during heating, the orthorhombic phase forms (for detailed temperatures see chapter 3.2).The diffractogram for the transition state shows that the peak splitting occurs for almost every α_2 peak. Obvious examples are the α_2-(20$\bar{2}$0) peak and the α_2-(20$\bar{2}$1) peak, where a shoulder has formed. However, what looks like the overlapping of two peaks is essentially the sum of three peaks. When the orthorhombic phase forms, the amount of α_2 decreases, and it comes to the overlapping with the corresponding peaks of the orthorhombic phase. Because of the structural similarities between the α_2 phase and the B19 and O phase, the positions of the peaks of the orthorhombic phases are close to the ones of the α_2 phase [12]. Due to the lower symmetry of the orthorhombic phase, however, more individual peaks are present in the diffraction pattern. So in the case of the α_2-(20$\bar{2}$0) and the α_2-(20$\bar{2}$1) peaks, which overlap with two peaks of the orthorhombic phase each, this double peak shape is formed.

When the temperature is raised above approximately 700 °C, the orthorhombic phase vanishes and γ is formed. This is in agreement with other reports in the literature, which suggest that the B19 phase is a transition phase from α_2 to γ. For example, Song et al. [18] observed the B19 phase as a transition phase between α_2 and γ in a Ti-45Al-8.5Nb-0.2W-0.2B-0.02Y (at.%) alloy. Tanimura et al. [22] found that the B19 phase, which had formed in the α/α_2 phase, acted as nucleation site for the γ phase in a binary Ti-40Al (at.%) alloy. In the present work, the diffraction data show that if the temperatures are high enough or the holding times are long enough so that the orthorhombic phase vanishes, a large amount of γ phase is formed. This indicates that the orthorhombic phase acts indeed as a transition phase between the α_2 and the γ phase also in the investigated Mo containing Ti-44.5Al-3.2Mo-0.1B (at.%) alloy. Along with the formed γ phase retained α_2 and β_o phase are present in the end state.

The amount of β_o phase, in contrast to the phase fraction of the other phases, is nearly constant throughout the experiments, which can be inferred from the small change in the height of the β_o-(110) main peak (Fig. 2). Also Rietveld analysis proves that the maximum difference in the β_o phase fraction between the different states is only 5 vol.%. However, the β_o-(100) superstructure

peak, which is already small in the water-quenched state (Fig. 2a), decreases during heating and is almost invisible in the end state (Fig. 2c). The β_o-(100) peak is shown at a higher magnification in Fig. 2 for each state to highlight this fact. The decrease in height can be attributed to the diffusion of molybdenum. Because of the water quenching the amount of molybdenum in the α_2' martensite and the β_o phase is roughly the same in the water-quenched state. Due to the elevated temperatures during the experiments a part of this β-stabilizing element can partition to the β_o phase [5]. Molybdenum has a strong influence on the superstructure peaks, because a higher fraction of molybdenum in the β_o phase yields a decrease in the intensity of the corresponding superstructure reflections. This can be explained by the fact that molybdenum occupies the Al sublattice in the β_o phase [23]. Therefore, the difference in the electron densities of the Ti sublattice and the Al sublattice becomes smaller and so does the intensity of the superstructure reflections.

3.2. Rietveld analysis and characterization of the orthorhombic phase

For a good Rietveld refinement of the diffraction data an accurate model for each phase is essential. This model needs the information of the crystal structure and the position of the atoms in the unit cell. These data can be found in literature, for example, see Ref. [3]. Regarding the site occupation of the atomic sites in the lattice, it has to be considered that the fast cooling leads to phases far from thermodynamic equilibrium. Therefore, the chemical composition of each phase is of great importance. Thus, EDX measurements were carried out in the TEM. Several measurements were performed for each phase and the average compositions are given in the following. In the water-quenched state the α_2 laths have a chemical composition of 54.6Ti-42.4Al-3.0Mo (at.%). As mentioned in chapter 3.1, the region between the α_2 laths consists of β_o phase and α_2' martensite. The TEM investigations have shown that they form very fine structures and, therefore, it was not possible to measure the chemical compositions of the two phases individually. So the result of the EDX measurements, which is 56.2Ti-40.6Al-3.2Mo (at.%), is a weight mean of their real composition. But due to the nature of the martensitic transformation the composition of these two phases should be the same in any case. The same problem connected with fine structures occurred for the α_2 phase

and the orthorhombic phase in the transition state. The EDX measurements for the combination of these two phases with the laths yield 54.3Ti-42.4Al-3.3Mo (at.%). The composition of the β_o phase, the α_2' martensite and the orthorhombic phase is 57.3Ti-38.6Al-4.1Mo (at.%). For the end state the EDX results after the HIP process are used, because in this state the samples approach a near-equilibrium condition. The chemical composition of the α_2 phase is 66.1Ti-31.3Al-2.6Mo (at.%) and of the β_o phase 56.2Ti-36.1Al-7.7Mo (at.%). For the chemical composition of the γ phase the EDX measurements yield 52.2Ti-46.3Al-1.5Mo (at.%).

Now the site occupancy factors of titanium, aluminum and molybdenum on the sublattices have to be adjusted according to this information. Holec et al. [23] have performed first principle calculations regarding the preferential site occupation of the early transition metals. They found that molybdenum prefers to occupy the Ti sublattice in the α_2 and the γ phase, but the Al sublattice in the β_o phase. For the B19 phase the Ti sublattice is slightly preferred [23]. On the basis of these findings the site occupancy factors, which are needed for the Rietveld refinement, were established using the EDX results as initial values. In Tab. 1 the adjusted site occupancy factors of titanium, aluminum and molybdenum for the titanium and aluminum sublattices of each phase in the three different states are shown. The orthorhombic phase is represented by the B19 phase. The molybdenum content increases in the β_o phase, whereas it decreases in the α_2 phase during the heating and ageing experiments. This is in agreement with the decrease in height of the β_o superstructure peak at a relatively constant β_o amount (see chapter 3.1). However, the occurring α_2' martensite influences the adjusted site occupancy factors. As the α_2' martensite and the α_2 phase cannot be distinguished in the diffraction data, the overall adjusted factors are a weight mean of the ones of the α_2 phase and the α_2' martensite.

Regarding the Rietveld refinement some additional points have to be considered. First, to get a good refinement the diffraction data should consist of smooth rings for each phase and not only some spots from single large grains [24]. Figure. 1 shows that in every state rings are present and that grain statistics are satisfactory. Second, because the α_2' martensite and the α_2 phase share the

same crystal structure, they cannot be distinguished in the diffraction data [4]. So the results of the Rietveld refinement are only valid for a combination of both of them.

For the orthorhombic phase, we choose the model of the B19 structure. From a crystallographic point of view, a transformation of the α_2 phase directly into the B19 phase is not possible [25]. If the α_2 phase, the B19 phase and the O phase are modeled in their largest common subgroup Cmcm (see Ref. [12]), in the case of the α_2 phase the Wyckoff positions 8g and 4c1 show the same site occupancy. For the B19 phase the site occupancies of 4c1 and 4c2 are the same, but the one of the 8g position is different. So for the transformation $\alpha_2{\rightarrow}$B19 the site occupancy of the Wyckoff position 4c1 has to change. This yields an intermediate state, in which all three Wyckoff positions have a different occupancy, which results in the structure of the O phase. Therefore, it is only possible for the O phase to form directly from the α_2 phase. However, for the following Rietveld analysis of the synchrotron diffraction data the B19 phase was used for several reasons. First, it is the simplest model of an orthorhombic phase. Furthermore, well-founded information regarding the site occupancy of the sublattices only exit for the B19 phase (see Ref. [23]) but not for any other orthorhombic model. Figure 3 indicates the good quality of the Rietveld refinement using this model.

Setting the B19 structure as the orthorhombic structure in the Rietveld refinement, it is now possible to evaluate the diffraction data of all three materials conditions in terms of phase fractions, lattice parameters and site occupancy factors. The results of the refinement on the basis of the data given in Tab. 1 for each phase are shown in Tab. 2. The upper part shows the lattice parameters for each phase at room temperature. The lattice parameters for the B19 phase are a=4.615 Å, b=2.920 Å and c=4.889 Å. Abe et al. [8], who reported on the B19 phase in a binary Ti-48Al (at.%) alloy, obtained a=4.5 Å, b=2.8 Å and c=4.9 Å at room temperature. The small differences could be related to the different chemical compositions or evaluation techniques. It should be noted that these authors estimated the lattice parameters from selected area diffraction patterns, whereas in this work they are evaluated using Rietveld refinement of diffraction data. Furthermore, the lattice parameters for the B19 phase were evaluated at 650 °C, which results in a=4.647 Å, b=2.935 Å and c=4.934 Å.

Schmoelzer et al. [11] determined for the B19 phase a=4.65 Å, b=2.93 Å and c=4.95 Å at a temperature of 640 °C, which agree well with the refined lattice parameters in this work. Assuming an enlarged unit cell according to the largest common subgroup Cmcm the values are also close to those reported by Rackel et al. [12]. Also for the other phases the lattice parameters are in good agreement with the literature [3]. It should be noted that the lattice parameters of the α_2 and the β_o phase are slightly different in each state. This can be attributed to the change in the phase composition.

The phase fractions for each phase in the different states are shown in the lower part of Tab. 2. It should be mentioned at this point that the refinement of the phase fractions is very sensitive to grain statistics. Thus, the small sample size and the very weak texture may have an influence on the accuracy of the phase fractions, but both factors could not be corrected for the available data. The amount of α_2/α_2' phase decreases significantly from 85 vol.% in the water-quenched state to 36 vol.% when the orthorhombic phase is formed in the transition state. After the dissolution of this phase the microstructure contains 74 vol.% γ, 11 vol.% α_2/α_2' and 15 vol.% β_o in the end state. Regarding the amount of β_o phase only a minor change from 15 vol.% to a minimum of 10 vol.% can be observed throughout the measurement, which agrees with the already mentioned relatively constant height of the β_o-(110) peak.

Analyzing the *in situ* synchrotron radiation experiments some additional statements about the orthorhombic phase can be made. Figure. 4 shows the azimuthally integrated intensities for selected temperatures during an *in situ* heating and cooling experiment. The temperature was raised from 500 °C to 800 °C at a heating rate of 2 K/min and subsequently decreased again from 800 °C to 500 °C at the same cooling rate. In Figs. 4a, 4b and 4c three diffractograms corresponding to different temperatures during the heating part are given. They represent the water-quenched state (Fig. 4a), the transition state (Fig. 4b) and the end state (Fig. 4c) during the *in situ* experiment. In Figs. 4d, 4e and 4f the diffractograms for the same temperatures during the cooling step are shown. Upon cooling, the amount of γ increases up to 70 vol.%, whereas the amount of α_2 decreases to 20 vol.%.

By comparing the height of the α_2-(20$\bar{2}$1) and γ-(111) peak in the diffractogram at 750 °C during heating (Fig. 4c) and in the first diffractogram during cooling also at 750 °C after the maximum temperature of 800 °C was reached (Fig. 4d), it is obvious that the γ peak has increased, whereas the α_2 peak has decreased. However, it is interesting to note that during cooling no orthorhombic phase is formed. Additional *in situ* experiments conducted at a lower heating/cooling rate of 0.5 K/min also confirm this finding. Therefore, the formed orthorhombic phase must be a metastable transition phase for the α_2/γ transformation, which only forms upon reheating after the water quenching. This finding is also in agreement with literature [8,22].

Furthermore, the formation and dissolution temperatures of the orthorhombic phase can be evaluated from the *in situ* measurements. They are defined as the temperatures, at which the peak width of the α_2 peaks starts to increase due to the formation of the orthorhombic phase. In Tab. 3 the formation and dissolution temperatures for the heating experiments as well as the formation and dissolution time for the ageing experiments are given. At a heating rate of 2 K/min the orthorhombic phase forms at 590 °C and dissolves at 724 °C. When a lower heating rate of 0.5 K/min is applied the formation starts at 580 °C and then the orthorhombic phase is present until 710 °C is reached. In the literature similar temperature intervals can be found for the orthorhombic phase. For example, Rackel et al. [12] found in a Nb-containing γ-TiAl based alloy a similar temperature interval from 550 °C to 700 °C for the O phase. Schmoelzer et al. [11] found in a Mo-containing alloy variant that the B19 phase is formed in a temperature range from 600 °C to 700 °C when a heating rate of 2 K/min is applied. Differences may stem from the method with which the formation and dissolution temperatures are evaluated. At the higher cooling rate of 2 K/min the temperature, interval is shifted to higher temperatures because the formation of the orthorhombic phase is a diffusional process. This is supported by the fact that the splitting of the peaks changes continuously during the measurements. The ageing experiments show that a higher annealing temperature reduces the time necessary for the formation of the orthorhombic phase. For 600 °C the orthorhombic phase occurs two minutes after reaching the annealing temperature. For the ageing at 700 °C the orthorhombic

phase forms already during the heating process. The 650 °C ageing test lies between these two. This finding can be attributed to the dependence of diffusion on temperature. At higher temperatures the time needed to form a sufficient amount of orthorhombic phase, which can be detected via diffraction, is decreased. For the dissolution times no comparison between the ageing experiments is possible because the ageing time at 600 °C and 650 °C was too short.

3.3. TEM investigations of the microstructure

As mentioned in chapter 3.1 the resolution of the SEM images shown in Fig. 1 is too low to reveal changes in the microstructure. In all states (water-quenched, transition and end) it consists of large α_2 laths or needles with a mixture of phases in between. The synchrotron diffraction data, however, indicate a significant change of the occurring phases. Therefore, TEM investigations were performed and correlated to the synchrotron diffraction data. The results are shown in Fig. 5, in which each of the three columns represents one state. Figures 5a, 5b and 5c show an overview image of the microstructure obtained by SEM. In the lower two rows the TEM images of the α_2' martensite region and the α_2 laths are shown for the corresponding state. Figures 5d, 5e and 5f represent the phase mixture region. In contrast, Figs. 5g, 5h and 5i the large α_2 laths. The first column of TEM images corresponds to the water-quenched state. At this magnification the α_2' martensite is clearly visible with an acicular structure, which was also reported by Mayer et al. [4]. The β_o phase is present between the martensitic needles. The large laths in Fig. 5d are essentially the α_2 phase, which can be concluded from the synchrotron data and the SAED data (not shown here). When comparing the water-quenched state with the transition state, the change in the microstructure becomes visible. Lamellae have formed in the large α_2 laths and in the α_2' martensite (Figs. 5e and 5h). These lamellae are essentially the orthorhombic phase. Within the α_2 lamellae a modulation of the contrast is visible. This corresponds to a so-called modulated microstructure. Such a microstructure was reported by Appel et al. [16,17] to occur in a Ti-(40-44)Al-8.5Nb (at.%) alloy, in which the B19 phase occurred. The modulated microstructure was also reported for alloys which contain the O phase, for example by Gabrisch et al. [13]. Additionally, it is interesting to note that the orthorhombic phase has also

14

formed within the α_2' martensite, which can be seen in Fig. 5e. This can be explained by the fact that α_2 and α_2' have the same crystal structure and that the difference in their chemical composition is rather small, when their thermal history is condsidered. However, to the best of the authors' knowledge the formation of an orthorhombic phase in the α_2' martensite has not been reported in the literature yet. The lamellae, which are visible in Figs. 5f and 5i after the orthorhombic phase has vanished, are essentially formed by the γ phase in α_2. They are present within the large laths as well as in the α_2' martensite. Their size is comparable with the lamellae of the orthorhombic phase and no contrast modulation is visible. A similar behavior for the γ phase was reported by Cha et al. [26] in an oil-quenched Ti-45Al-7.5Nb (at.%) alloy. These authors found that the γ phase formed nanometer-scaled lamellae in the α_2 phase during an annealing treatment after an oil quenching from the single α phase field region. But in contrast to the alloy studied by Cha et al. [26], in which the γ phase formed directly out of the α_2 phase, in the present work the γ phase formed via the orthorhombic transition phase.

4. Conclusion

Using *in situ* HEXRD and TEM a β-homogenized and quenched Ti-44.5Al-3.2Mo-0.1B (at.%) alloy was studied regarding the evolution of the microstructure and the formation of an orthorhombic phase during reheating. Upon reheating this phase formed a modulated microstructure upon heating inside the α_2 laths as well as in the α_2' martensite, which could be revealed by TEM. The occurrence of such a microstructure due to the formation of an orthorhombic phase is in agreement with literature. Additionally, the *in situ* experiments showed that this phase is metastable and only present in a temperature interval from approximately 600 °C to 720 °C. However, it was not possible to determine if the formed orthorhombic phase is the O phase or the B19 phase. As the formation of γ occurs simultaneously with the dissolution of the orthorhombic phase it can be concluded that the orthorhombic phase acts as a transition phase between the α_2 and the γ phase. However, to fully

understand the chemical regime and to identify the type of the orthorhombic phase in Mo-containing γ-TiAl based alloys, further investigations are needed.

5. Acknowledgment

References

[1]   H. Kestler, H. Clemens, Production, processing and application of γ(TiAl)-based alloys, in: M. Peters, C. Leyens (Eds.), Titanium and titanium alloys: fundamentals and applications, Wiley-VCH Verlag, Weinheim, 2003: pp. 351–393.

[2]   H. Clemens, S. Mayer, Intermetallic titanium aluminides as innovative high temperature lightweight structural materials-How materialographic methods have contributed to their development, Pr. Met. 52 (2015) 691–721. doi:10.3139/147.110366.

[3]   A. Stark, Textur- und Gefügeentwicklung bei der thermomechanischen Umformung Nb-reicher γ-TiAl-Basislegierungen, PhD. Thesis, Shaker Verlag, Aachen, 2010.

[4]   S. Mayer, M. Petersmann, F.D. Fischer, H. Clemens, T. Waitz, T. Antretter, Experimental and theoretical evidence of displacive martensite in an intermetallic Mo-containing γ-TiAl based alloy, Acta Mater. 115 (2016) 242–249. doi:10.1016/j.actamat.2016.06.006.

[5]   H. Clemens, S. Mayer, Design, processing, microstructure, properties, and applications of advanced intermetallic TiAl alloys, Adv. Eng. Mater. 15 (2013) 191–215. doi:10.1002/adem.201200231.

[6]   D. Banerjee, A.K. Gogia, T.K. Nandy, V.A. Joshi, A new ordered orthorhombic phase in a Ti_3Al-Nb alloy, Acta Metall. 36 (1988) 871–882. doi:10.1016/0001-6160(88)90141-1.

[7]   K. Muraleedharan, T.K. Nandy, D. Banerjee, S. Lele, Phase stability and ordering behaviour of the O phase in TiAlNb alloys, Intermetallics 3 (1995) 187–199. doi:10.1016/0966-9795(95)98930-7.

[8]   E. Abe, T. Kumagai, M. Nakamura, New ordered structure of TiAl studied byhigh-resolution electron microscopy, Intermetallics 4 (1996) 327–333. doi:10.1016/0966-9795(95)00051-8.

[9]   D. Banerjee, The intermetallic Ti_2AlNb, Prog. Mater. Sci. 42 (1997) 135–158. doi:10.1016/S0079-6425(97)00012-1.

[10]   F.A. Sadi, C. Servant, On the B2→O phase transformation in Ti–Al–Nb alloys, Mater. Sci. Eng. A 346 (2003) 19–28. doi:10.1016/S0921-5093(02)00507-5.

[11]   T. Schmoelzer, A. Stark, E. Schwaighofer, T. Lippmann, S. Mayer, H. Clemens, In situ synchrotron study of B19 phase formation in an intermetallic γ-TiAl alloy, Adv. Eng. Mater. 14 (2012) 445–448. doi:10.1002/adem.201200047.

[12]   M.W. Rackel, A. Stark, H. Gabrisch, N. Schell, A. Schreyer, F. Pyczak, Orthorhombic phase formation in a Nb-rich γ-TiAl based alloy – An in situ synchrotron radiation investigation, Acta Mater. 121 (2016) 343–351. doi:10.1016/j.actamat.2016.09.030.

[13]   H. Gabrisch, U. Lorenz, F. Pyczak, M. Rackel, A. Stark, Morphology and stability of orthorhombic and hexagonal phases in a lamellar γ-Ti-42Al-8.5Nb alloy - A transmission electron microscopy study, Acta Mater. 135 (2017) 304–313. doi:10.1016/j.actamat.2017.05.067.

[14]   G. dong Ren, J. Sun, High-resolution electron microscopy characterization of modulated structure in high Nb-containing lamellar γ-TiAl alloy, Acta Mater. 144 (2018) 516–523. doi:10.1016/j.actamat.2017.11.016.

[15]   F. Appel, M. Oehring, J.D.H. Paul, Nano-scale design of TiAl alloys based on β-phase decomposition, Adv. Eng. Mater. 8 (2006) 371–376. doi:10.1002/adem.200600013.

[16]   F. Appel, M. Oehring, J.D.H. Paul, A novel in situ composite structure in TiAl alloys, Mater. Sci. Eng. A 493 (2008) 232–236. doi:10.1016/j.msea.2007.08.095.

[17]   F. Appel, J.D.H. Paul, M. Oehring, Phase transformations during creep of a multiphase TiAl-based alloy with a modulated microstructure, Mater. Sci. Eng A 510–511 (2009) 342–349. doi:10.1016/j.msea.2008.08.047.

[18]   L. Song, X.J. Xu, L. You, Y.F. Liang, J.P. Lin, B19 phase in Ti–45Al–8.5Nb–0.2W–0.2B–0.02Y alloy, J. Alloys Compd. 618 (2015) 305–310. doi:10.1016/j.jallcom.2014.08.137.

[19]   P. Staron, T. Fischer, T. Lippmann, A. Stark, S. Daneshpour, D. Schnubel, E. Uhlmann, R. Gerstenberger, B. Camin, W. Reimers, E. Eidenberger-Schober, H. Clemens, N. Huber, A. Schreyer, In situ experiments with synchrotron high-energy X-rays and neutrons, Adv. Eng. Mater. 13 (2011) 658–663. doi:10.1002/9783527684489.ch20.

[20]   A.P. Hammersley, FIT2D: a multi-purpose data reduction, analysis and visualization program, J. Appl. Crystallogr. 49 (2016) 646–652. doi:10.1107/S1600576716000455.

[21]   L. Lutterotti, Total pattern fitting for the combined size-strain-stress-texture determination in thin film diffraction, Nucl. Instruments Methods Phys. Res. Sect. B 268 (2010) 334–340. doi:10.1016/j.nimb.2009.09.053.

[22]   M. Tanimura, Y. Inoue, Change in Al concentration profile related to the $DO_{19} \rightarrow L1_0$ structural change in Ti-Al alloys, Scr. Mater. 44 (2001) 365–373. doi:10.1016/S1359-6462(00)00573-X.

[23]   D. Holec, R.K. Reddy, T. Klein, H. Clemens, Preferential site occupancy of alloying elements in TiAl-based phases, J. Appl. Phys. 119 (2016) 1–8. doi:10.1063/1.4951009.

[24]   L.B. Mccusker, R.B. Von Dreele, D.E. Cox, D. Louër, P. Scardi, Rietveld refinement guidelines, J. Appl. Crystallogr. 32 (1999) 36–50. doi:10.1107/S0021889898009856.

[25]   L.A. Bendersky, A. Roytburd, W.J. Boettinger, Phase transformations in the $(Ti, Al)_3$ Nb section of the Ti-Al-Nb system—I. Microstructural predictions based on a subgroup relation between phases, Acta Metall. Mater. 42 (1994) 2323–2335. doi:10.1016/0956-7151(94)90311-5.

[26]   L. Cha, C. Scheu, H. Clemens, H.F. Chladil, G. Dehm, R. Gerling, A. Bartels, Nanometer-scaled

lamellar microstructures in Ti-45Al-7.5Nb-(0; 0.5)C alloys and their influence on hardness, Intermetallics 16 (2008) 868–875. doi:10.1016/j.intermet.2008.03.009.

Tables

Table 1: Adjusted site occupancy factors of titanium, aluminum and molybdenum for each phase as used in the Rietveld analysis. For the orthorhombic phase the results of the B19 phase are shown. Occupancy factors of the titanium and aluminum sublattice are only shown when the corresponding phase was present in this state. At the top, the sublattices within each phase are additionally defined by their Wyckoff positions.

Phase		α_2			β_o			γ			B19		
Wyckoff positions	Ti lattice	6h			1a			2e			2e		
	Al lattice	2d			1b			1a, 1c			2f		
Elements		Ti	Al	Mo	Ti	Al	Mo	Ti	Al	Mo	Ti	Al	Mo
Water-quenched state (at.%)	Ti lattice	69.5	26.5	4.0	83.3	16.7	0.0	-	-	-	-	-	-
	Al lattice	10.0	90.0	0.0	29.1	64.5	6.4	-	-	-	-	-	-
Transition state (at.%)	Ti lattice	69.1	26.5	4.4	100	0.0	0.0	-	-	-	91.5	5.0	3.5
	Al lattice	10.0	90.0	0.0	14.7	77.2	8.1	-	-	-	16.7	80.3	3.0
End state (at.%)	Ti lattice	84.8	11.7	3.5	100	0.0	0.0	97.0	0.0	3.0	-	-	-
	Al lattice	10.0	90.0	0.0	12.4	72.2	15.4	7.4	92.6	0.0	-	-	-

Table 2: Results of the Rietveld refinement. The lattice parameters of α_2 and β_o are given for the water-quenched (WQ) state. The lattice parameters for the γ phase correspond to the end state, the ones for the B19 phase to the transition state. All lattice parameters were determined at room temperature. The lower part of Tab. 2 shows the phase fractions for the three states at room temperature after the annealing treatments described in chapter 2. It should be noted that α_2 corresponds to both the α_2 laths and the α_2' martensite in the specimens.

		α_2	β_o	γ	B19
Lattice constant (Å)	a	5.748	3.202	4.054	4.615
	b	-	-	-	2.920
	c	4.616	-	4.086	4.889
WQ state (vol.%)		85	15	0	0
Transition state (vol.%)		36	10	0	54
End state (vol.%)		11	15	74	0

Table 3: Formation and dissolution of the orthorhombic phase. For the *in situ* heating experiments the formation and dissolution temperatures of the orthorhombic phase are given for two heating rates. Also for the *in situ* isothermal ageing experiments the formation and dissolution times have been evaluated.

Heating experiment	Formation temperature (°C)	Dissolution temperature (°C)
400 °C to 900 °C at 2 K/min	590	724
575 °C to 720 °C at 0.5 K/min	575	700
Ageing experiments	**Formation time (sec)**	**Dissolution time (sec)**
600 °C for 8 h	120	-
650 °C for 2 h	15	-
700 °C for 2 h	During heating	1443

Figures
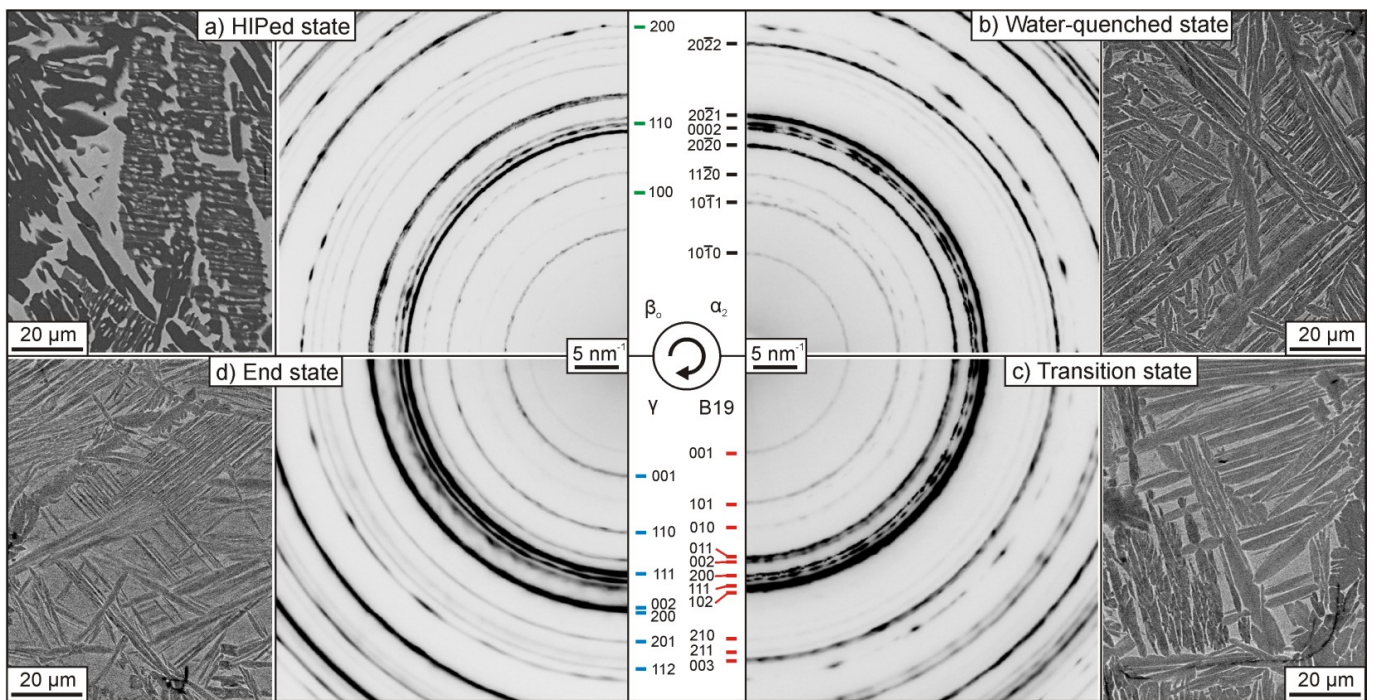
Figure 1: Sections of the two-dimensional diffraction patterns at room temperature and the corresponding microstructures of the Ti-44.5Al-3.2Mo-0.1B (at.%) alloy. All SEM images were taken in BSE mode. In the center peak positions of the α_2 (black), the β_o (green), the γ (blue) and the B19 phase (red), which is used as the orthorhombic phase, are marked. Panel (a) corresponds to the HIPed state. In the SEM micrograph the γ phase has a dark gray to black contrast, the β_o phase a light gray contrast and the α_2 phase shows a gray contrast. Panel (b) shows the water-quenched state, (c) the transition state and (d) the end state. In these SEM images the dark lath-like structures are the α_2 phase and the areas with the brighter contrast in between are a mixture of α_2' martensite and β_o phase.
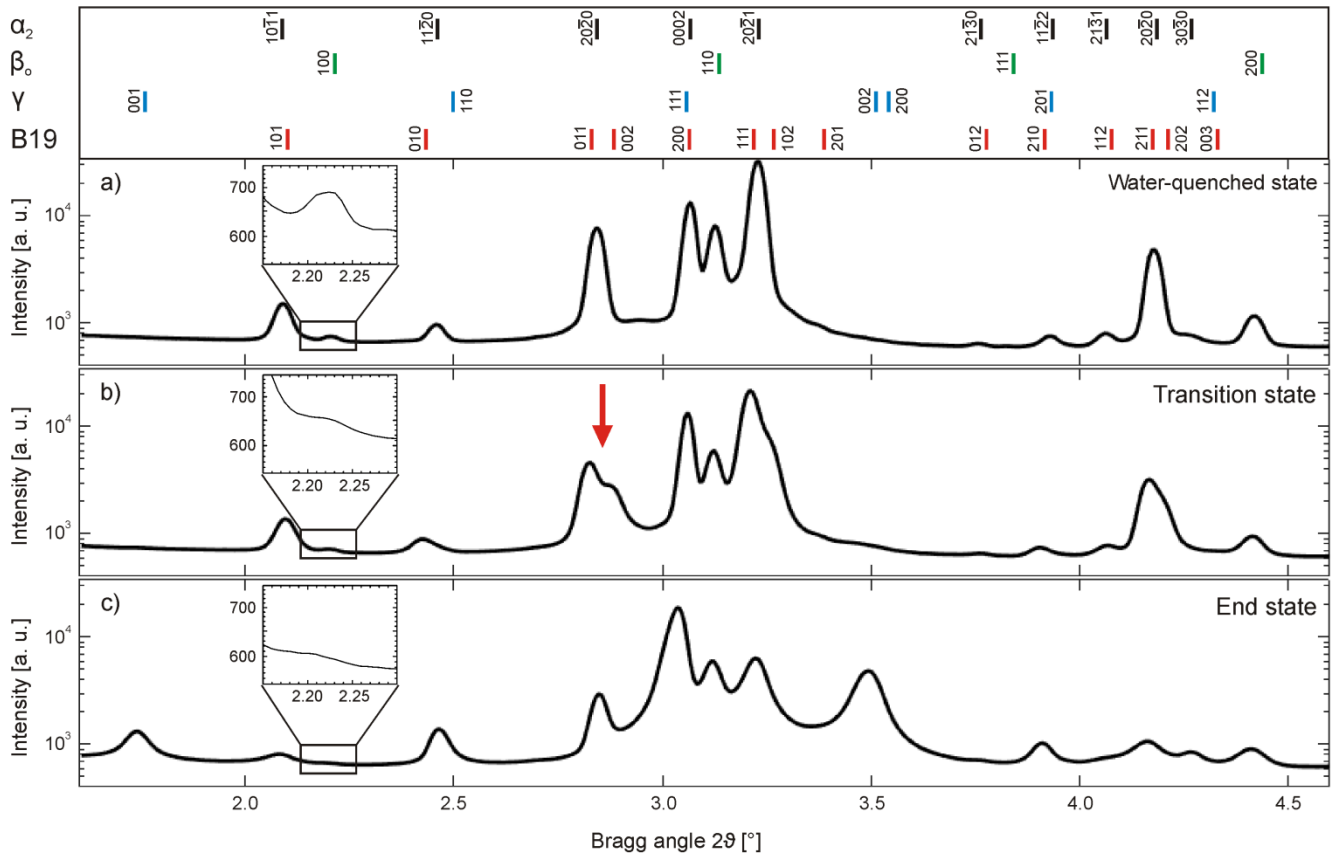
Figure 2: Azimuthally integrated intensities for the water-quenched state (a), the transition state (b) and the end state (c) are shown as a function of the Bragg angle 2ϑ at room temperature. At the top the peak positions of the α_2 (black), the β_o (green), the γ (blue) and the B19 phase (red), which is used as the orthorhombic phase, are marked. For each state the β_o-(100) peak is shown at a higher magnification. One can clearly see the peak splitting of the α_2 phase in the transition state. For example, the splitting of the α_2-($20\bar{2}0$) peak is marked with a red arrow. In the end state a significant amount of γ phase is present.
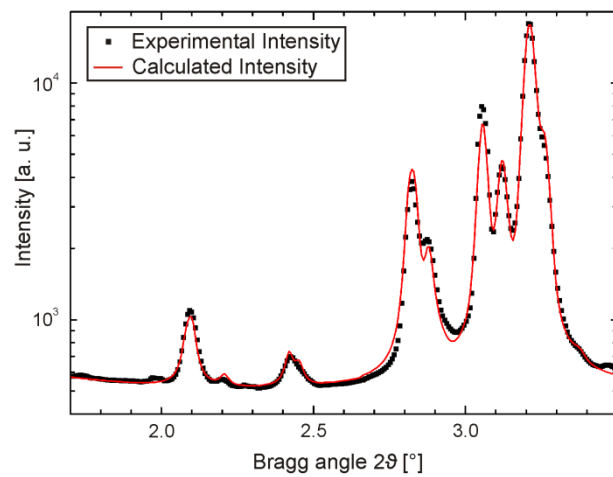
Figure 3: Rietveld refinement of the transition state using the B19 structure as model for the orthorhombic phase. Intensity calculated by the software MAUD (red line) and the intensity obtained in the synchrotron radiation experiments of the transition state (black squares).
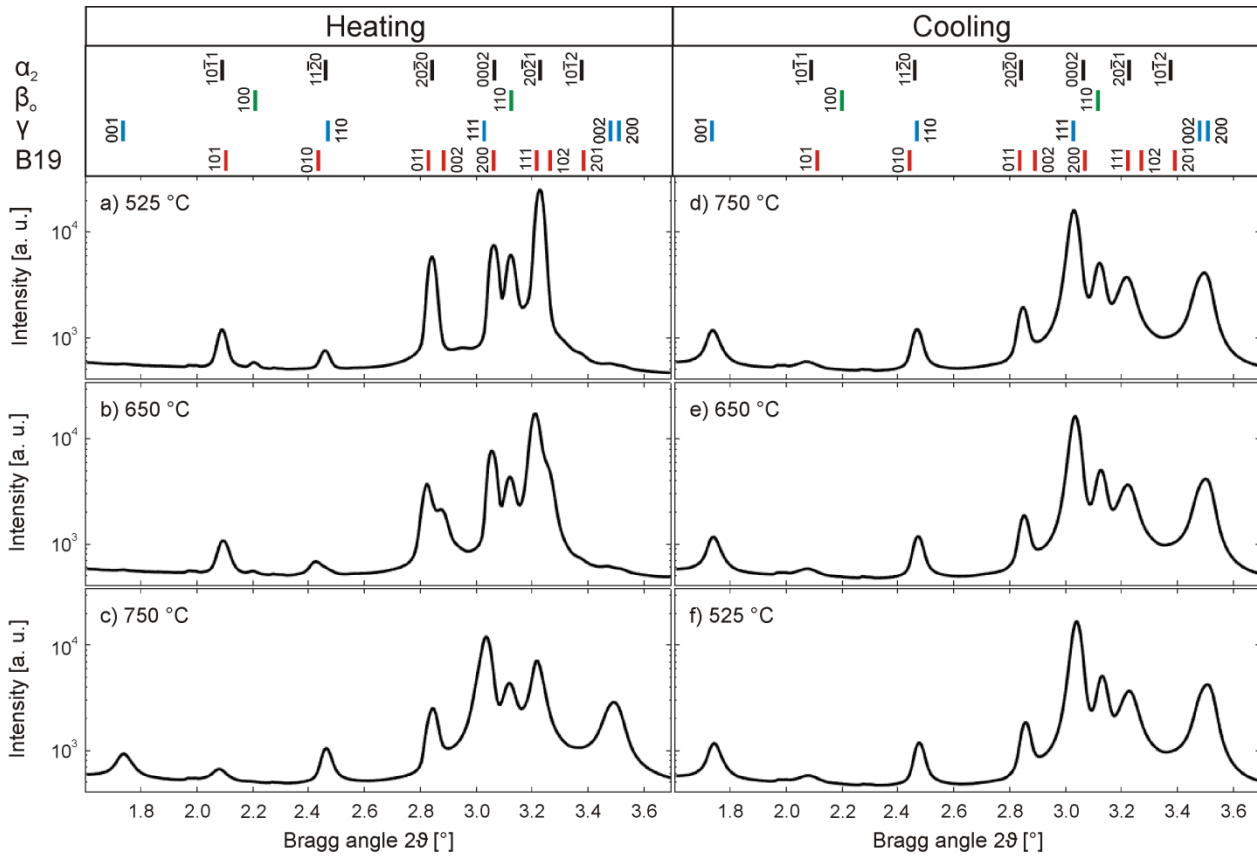
Figure 4: Indicated integrated diffraction patterns from the *in situ* heating and cooling experiment at the temperatures. The specimen was heated from 500 °C to 800 °C at a rate of 2 K/min and subsequently cooled to 500 °C again using the same rate. Panels (a), (b) and (c) show the diffractograms during the heating and panels (d), (e) and (f) during the cooling step. The corresponding temperatures are given in the top left corners in each diffractogram. At the top the peak positions for all four phases are marked. During the cooling sequence, no formation of the orthorhombic phase is visible.
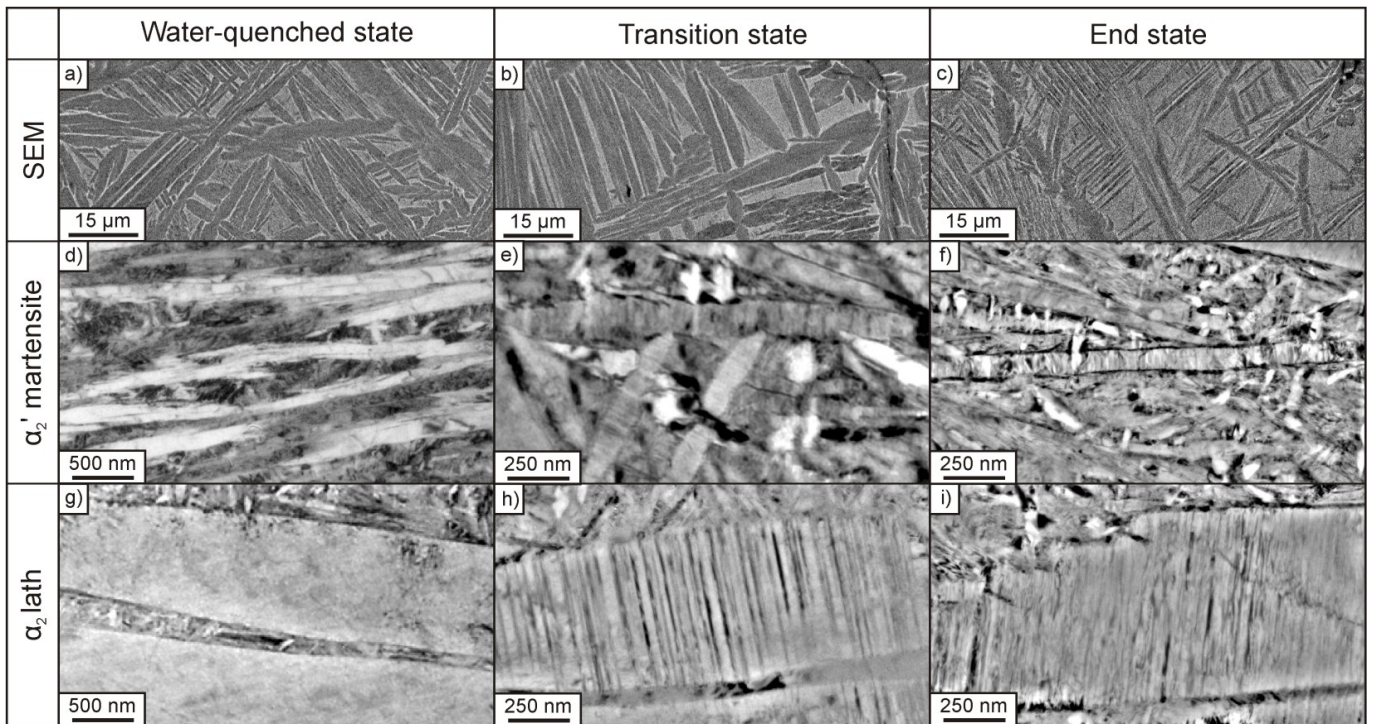
Figure 5: TEM images of the microstructure. In (a), (b) and (c) overview images of the microstructure obtained by SEM in BSE mode are given for each state. The images (a) to (i) show the TEM micrographs of the different parts of the microstructure. The α_2' martensite and β_o regions in the different states are shown in (d), (e) and (f). Panels (g), (h) and (i) show one large α_2 lath for each state. Especially in the α_2 lath the formed lamellae of the orthorhombic phase can be clearly seen in the transition state. In the end state the lamellae consist of γ phase.

Graphical Abstract